Linear and nonlinear optical properties of $In_xGa_{1-x}N/GaN$ heterostructures

Yong-Hoon Cho, T. J. Schmidt, S. Bidnyk, G. H. Gainer, and J. J. Song
Center for Laser and Photonics Research and Department of Physics, Oklahoma State University, Stillwater, Oklahoma 74078

S. Keller, U. K. Mishra, and S. P. DenBaars
Electrical and Computer Engineering and Materials Departments, University of California, Santa Barbara, California 93106
(Received 6 July 1999)

We have systematically studied both the spontaneous and stimulated emission properties in blue-light-emitting $In_xGa_{1-x}N/GaN$ multiple quantum well structures using various linear and nonlinear optical techniques. Our experimental observations are consistently understandable in the context of localization of carriers associated with large potential fluctuations in the $In_xGa_{1-x}N$ active regions and at heterointerfaces. The studies have been done as a function of excitation power density, excitation photon energy, excitation length, and temperature. The results show carrier localization features for spontaneous emission and demonstrate the presence of potential fluctuations in the $In_xGa_{1-x}N$ active region of the $In_xGa_{1-x}N/GaN$ structures and its predominant role in spontaneous emission. In addition, the experimental observations strongly indicate that the stimulated emission has the same microscopic origin as spontaneous emission, i.e., radiative recombination of localized states. Therefore, we conclude that carriers localized at potential fluctuations in $In_xGa_{1-x}N$ active layers and interfaces can play a key role in not only spontaneous but also stimulated emission of state-of-the-art blue-light-emitting $In_xGa_{1-x}N/GaN$ quantum structures.

I. INTRODUCTION

With the recent progress made in nitride growth technology, much research has been devoted to group-III nitride wide-gap semiconductors for their applications such as ultraviolet (UV)-visible light emitters, solar-blind UV detectors, and high-temperature and high-power electronic devices. In spite of poor structural quality (e.g., the large dislocation density) of nitride epitaxial layers compared to other III-V semiconductors, high-brightness light-emitting diodes[1] and cw blue laser diodes[2] based on $In_xGa_{1-x}N$ structures have been achieved with high performance and high quantum efficiency. Understanding the physical mechanisms giving rise to spontaneous emission (SPE) and stimulated emission (SE) in $In_xGa_{1-x}N$-based structures is crucial not only from the viewpoint of physical interest but also in designing practical devices. Although a wealth of SPE and SE studies in GaN-based quantum wells (QW's) (such as $In_xGa_{1-x}N/GaN$ and $GaN/Al_xGa_{1-x}N$) have been reported, the results in the literature are varied and controversial.

For SPE, it has been discussed that the built-in macroscopic polarization, which consists of the spontaneous polarization due to interface charge accumulations between two constituent materials and the piezoelectric polarization due to lattice-mismatch-induced strain,[3] plays a significant role in the wurtzite III-V nitrides system.[4] These polarization charges generate a *built-in internal electric field* (*IEF*) directed along the growth direction (perpendicular to the layers) and modify both electronic energy levels and wave functions. These internal polarization fields give rise to changes in optical matrix elements and can be screened by photogenerated electron-hole pairs. It has been argued that the spontaneous polarization and/or the strain-induced piezoelectric polarization play an important role in carrier recombination in both $GaN/Al_xGa_{1-x}N$ and $In_xGa_{1-x}N/GaN$ QW's.[5–7] Recombination of carriers localized at band-tail states of potential fluctuations has also been discussed as an important SPE mechanism in $In_xGa_{1-x}N/GaN$ QW's and even in $GaN/Al_xGa_{1-x}N$ QW's that exclude alloy fluctuations in the active region.[8–12] The inhomogeneous potential fluctuations can be caused by alloy composition fluctuation, well size irregularity, and/or other crystal imperfections such as point defects and dislocations, resulting in a spatial band-gap variation in the plane of the layers. The radiative recombination in $In_xGa_{1-x}N/GaN$ multiple QW's (MQW's) has also been attributed to emission from highly localized deep states originating from quantum dot-like and phase-separated In-rich regions in the wells.[13,14] This *carrier localization* (*CLO*) formed in the plane of the layers enhances the quantum efficiency by suppressing lateral carrier diffusion, thereby reducing the probability for carriers to enter nonradiative recombination centers.

For SE, there have been several attempts to account for the gain and lasing mechanism in III-V and II-VI semiconductors. Whereas *electron-hole plasma* (*EHP*) recombination is accepted as the gain mechanism in most III-V semiconductors, such as GaAs and InP, there is a debate over whether the SE in $In_xGa_{1-x}N$-based structures is caused mostly by EHP. A considerable amount of attention has been given to the potential role of strongly localized band-tail states in the SE and lasing processes in $In_xGa_{1-x}N$ MQW's. Although many data support CLO recombination as the mechanism leading to SPE in these materials, the results for SE behavior in the literature are varied and often controversial. This has led some research groups to assign the SPE peak to recombination of localized carriers, and the SE peak to a more traditional EHP recombination originating from free carriers, while others claim that recombination originating from strong CLO is the origin of both SPE and SE.

Ambiguities in the interpretation of some experimental

findings and a lack of direct experimental evidence make an unambiguous identification of the responsible SPE and SE mechanisms in $In_xGa_{1-x}N$ MQW's difficult, so controversies in the proposed emission mechanisms remain and a consistent model that properly describes the experimental observations is still not available. Accordingly, more direct experimental observations giving insight into several physical aspects, in addition to the traditional ones, are required to clarify the responsible recombination mechanism for both linear and nonlinear optical properties. In this paper, we present a comprehensive study of both the SPE and SE behaviors of $In_xGa_{1-x}N$/GaN MQW structures by means of a variety of optical techniques. We focus especially on optical characteristics of $In_xGa_{1-x}N$/GaN heterostructures with $x \sim 0.2$ used for state-of-the-art blue-light-emitting structures and $In_xGa_{1-x}N$ thin films with comparable x. For the study of SPE, we employed photoluminescence (PL), PL excitation (PLE), and time-resolved PL (TRPL) spectroscopy. For the study of SE, we carried out optically pumped SE, variable stripe gain, and nanosecond nondegenerate pump-probe spectroscopy. Furthermore, using these techniques, we have investigated the excitation power, excitation photon energy, excitation length, and temperature dependence of the emission from these materials. Combining the results of the above studies, we find only CLO in the $In_xGa_{1-x}N$ active regions provides an adequate explanation for the observed SPE and SE behavior of these materials.

This paper is organized as follows. Section II gives details about the sample structures and experimental conditions. In Sec. III, we present the experimental results to demonstrate that localized carriers indeed play a central role in SPE, SE, and the formation of gain in $In_xGa_{1-x}N$/GaN MQW structures. In Sec. IV, we compare and discuss the experimental results. Our conclusions are summarized in Sec. V.

II. EXPERIMENTS

The $In_{0.18}Ga_{0.82}N$/GaN (to be referred as InGaN/GaN hereafter) MQW structures used in this study were grown on *c*-plane sapphire substrates by metalorganic chemical vapor deposition (MOCVD). A set of samples, nominally identical apart from deliberate variations in the Si doping concentration, were grown specifically to study the influence of Si doping in the GaN barriers. The samples consisted of a GaN buffer layer (1.8 μm) and a 12-period multiple quantum well consisting of 3-nm-thick InGaN wells and 4.5-nm-thick GaN barriers, followed by a 100-nm-thick $Al_{0.07}Ga_{0.93}N$ (to be referred as AlGaN hereafter) capping layer. Trimethylgallium (TMGa), trimethylindium (TMIn), trimethylaluminum, and ammonia were used as the precursors and disilane was used as the *n*-type dopant. The growth temperatures of the GaN base layer, the superlattice (SL) region, and the AlGaN capping layer were 1050, 790, and 1040 °C, respectively. The TMGa and TMIn fluxes during the SL growth were 5 and 14 μmol/min, respectively, while the ammonia flow was held constant at 0.35 mol/min. The doping concentrations were obtained from secondary-ion mass spectroscopy and Hall measurements. The $In_{0.18}Ga_{0.82}N$ (to be referred as InGaN hereafter) epilayer used for comparison was grown by MOCVD at 800 °C on a 1.8-μm-thick GaN layer deposited at 1060 °C on *c*-plane sapphire substrates. The InGaN layer was 0.1 μm thick and capped by a 0.05-μm-thick GaN layer.

To evaluate the interface quality and structural parameters, such as the average In composition of the wells and the period of the SL, the samples were analyzed with high-resolution x-ray diffraction (HRXRD) using Cu $K\,\alpha_1$ radiation. The average In composition was measured by HRXRD, assuming Vegard's law. The angular distances between the satellite SL diffraction peaks and GaN (0002) reflections were obtained by $\omega-2\theta$ scans. The spectra clearly show higher-order satellite peaks indicating high interface quality and good layer periodicity. In addition, we observed that the MQW samples are fully pseudomorphic from symmetric and asymmetric reciprocal space mapping. The details of our HRXRD analysis were reported elsewhere.[15]

Low-density SPE properties were investigated by PL, PLE, and TRPL spectroscopy. PL spectra were measured using the 325-nm line of a 20-mW cw He-Cd laser. PLE experiments were performed using quasimonochromatic light dispersed by a $\frac{1}{2}$-m monochromator from a xenon lamp. TRPL measurements were carried out using a tunable picosecond pulsed laser system consisting of a cavity-dumped dye laser synchronously pumped by a frequency-doubled mode-locked Nd:YAG (yttrium aluminum garnet) laser as an excitation source and a streak camera for detection. The output laser pulses from the dye laser had a duration of less than 5 ps and were frequency doubled into the UV spectral region by a nonlinear crystal. The overall time resolution of the system was better than 15 ps.

Optically pumped SE was performed in side-pumping geometry where edge emission from the samples was collected into a Spex 1.0-m spectrometer and recorded by an optical multichannel analyzer or a UV-enhanced gated charge-coupled device (CCD). The third harmonic (355 nm) of an injection-seeded Nd:YAG laser with a pulse width of 6 ns and a repetition rate of 30 Hz was used as the pumping source. The laser beam was focused on the sample surface using a cylindrical lens to form an excitation spot in the form of a line.[16] The laser light intensity could be attenuated continuously using a variable neutral density filter.

For the optical gain measurements, the variable stripe excitation length method was used.[17,18] The samples were optically excited by the third harmonic (355 nm) of an injection seeded, *Q*-switched Nd:YAG laser [$\sim$5 ns full width at half maximum (FWHM), 10 Hz repetition rate]. The excitation beam was focused to a line on the sample surface using a cylindrical lens and the excitation length was precisely varied using a mask connected to a computer-controlled stepper motor. The emission was collected from one edge of the samples, coupled into a $\frac{1}{4}$-m spectrometer, and spectrally analyzed using a UV-enhanced CCD. The modal gain $g_{mod}(E)$ at energy E is extracted from

$$\frac{I_1(E,L_1)}{I_2(E,L_2)}\,\frac{\exp[g_{\mathrm{mod}}(E)L_1]-1}{\exp[g_{\mathrm{mod}}(E)L_2]-1}$$

with $L_{1,2}$ two different stripe excitation lengths and $I_{1,2}$ the measured emission intensities. Special care was taken to avoid gain saturation effects in the optical gain spectra, so that the gain spectra are measured for stripe lengths shorter than those for which saturation effects occur.

For the nanosecond nondegenerate optical pump-probe experiments, the third harmonic of the Nd:YAG laser described above (355 nm) was used to synchronously pump the individual samples and a dye solution. The superradiant emission from the dye solution (covering the entire spectral range of the localized states) was collected and focused onto the samples, coincidental with the pump beam. The intensity of the probe was kept several orders of magnitude lower than the pump beam to avoid any nonlinear effects due to the probe. The spot size of the probe was kept at $\sim\frac{1}{3}$ that of the pump to minimize the role of variations in the pump intensity across the excitation spot. The transmitted (broadband) probe (with and without the pump beam) was then collected and coupled into a $\frac{1}{4}$-m spectrometer and spectrally analyzed using a UV-enhanced, gated CCD. The samples were mounted on a copper heat sink attached to a wide temperature range cryostat/heater system.

For the energy selective PL study, the second harmonic of a mode-locked Ti:sapphire laser was used as a tunable excitation source to excite the sample normal to the sample surface. The emission was collected normal to the sample surface, coupled into a 1-m spectrometer, and spectrally analyzed using a CCD. For energy selective SE experiments, the second harmonic of an injection-seeded, *Q*-switched Nd:YAG laser (532 nm) was used to pump an amplified dye laser. The deep-red to near-infrared radiation from the dye laser was frequency doubled in a nonlinear crystal to achieve the near-UV to violet laser radiation needed to optically excite the $In_xGa_{1-x}N$/GaN MQW's in the spectral region of interest. The frequency-doubled radiation ($\sim$4 ns pulse width, 10 Hz repetition rate) was focused to a line on the sample surface. The excitation spot size was approximately 100×5000 μm. The emission from the sample was collected from one edge of the sample, coupled into a 1-m spectrometer, and spectrally analyzed using a UV-enhanced CCD.

III. RESULTS

A. General optical characteristics

Figure 1 shows typical PL, PLE, and TRPL data of the InGaN-related emission with a peak energy of $\sim$2.8 and $\sim$2.99 eV at 10 K for (a) an InGaN/GaN MQW and (b) an InGaN epilayer, respectively. The 10-K near-band-edge emission from the AlGaN cladding layer [in (a)] and the GaN layers [in (a) and (b)] are also clearly seen at 3.60 and 3.48 eV, respectively. For the PLE detection energy of the InGaN-related emission peak, the contributions from the GaN layers [in (a) and (b)] and from the AlGaN capping layer [in (a)] are clearly distinguishable, and the energy positions of the absorption edge are well matched to the PL peak positions. The absorption of the InGaN wells in the MQW increases monotonically, reaching a maximum at $\sim$3.1 eV, and remains almost constant until absorption by the GaN barriers occurs at 3.48 eV. A large Stokes shift of this InGaN-related SPE peak with respect to the absorption edge measured by low power PLE spectroscopy is clearly observed for both samples. The band-tail states responsible for the ''soft'' absorption edge are seen to be significantly larger in the MQW than in the epilayer, as is the resulting Stokes shift of the SPE peak. This is most likely due to the increased number of interfaces in the MQW compared to the epilayer, which can lead to larger potential fluctuations. The temporal dynamics of the luminescence were also measured using the TRPL technique. The effective recombination lifetime as a function of detection energy across the 10-K PL spectrum of (a) the InGaN/GaN MQW and (b) the InGaN epilayer is also shown in Fig. 1. It should be noted that the rise in the effective lifetime τ with decreasing emission energy across the PL spectrum, resulting in a redshift behavior of the emission peak energy as time progresses, gives favorable evidence that the InGaN-related emission is due to radiative recombination of carriers localized at potential fluctuations. It is well known that the recombination of localized carriers is governed not only by radiative recombination but also by the transfer to and trapping in the energy tail states.[14,19] The differences in τ between the two samples indicate that the potential fluctuations localizing the carriers are significantly smaller in the epilayer than in the MQW. The SPE peak is attributed to radiative recombination of localized states in an analysis along the same vein as Narukawa *et al.*[14] We note that the observed longer lifetime for the MQW's compared to those reported by other groups is probably due to relatively larger degree of carrier localization caused by a larger number of QW's and/or different growth conditions used in this work.[8,20–22]

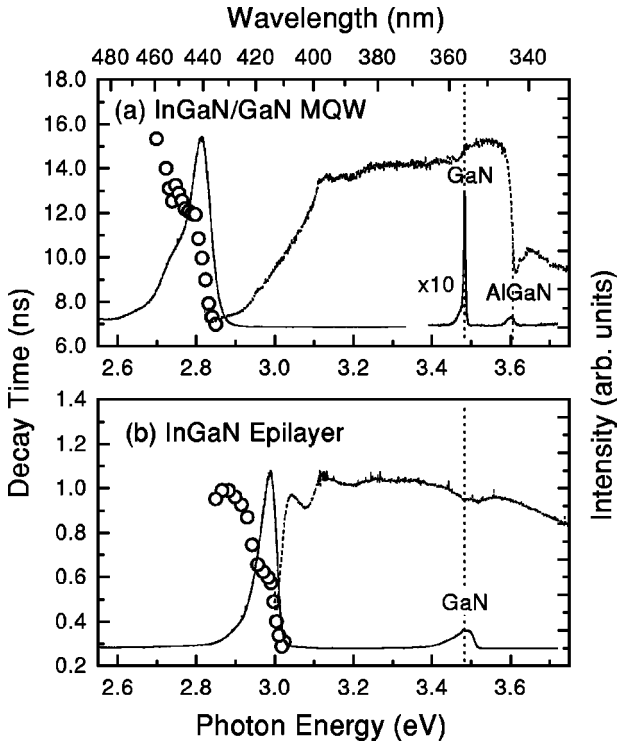

FIG. 1. 10-K PL (solid lines), PLE (dashed lines), and TRPL (open circles) data for (a) an InGaN/GaN MQW and (b) an InGaN epilayer. Both were grown by MOCVD on *c*-plane sapphire. A large Stokes shift of the PL emission from the InGaN layers with respect to the band-edge measured by PLE spectra is observed. The near-band-edge emission from the GaN and AlGaN layers was observed at 3.48 and 3.6 eV, respectively. The PLE contributions from the GaN layers [in (a) and (b)] and the AlGaN layer [in (a)] are clearly seen. A rise in lifetime with decreasing emission energy, resulting in a redshift behavior of the emission with time, reflects that the InGaN-related emission is due to radiative recombination of carriers localized at potential fluctuations.

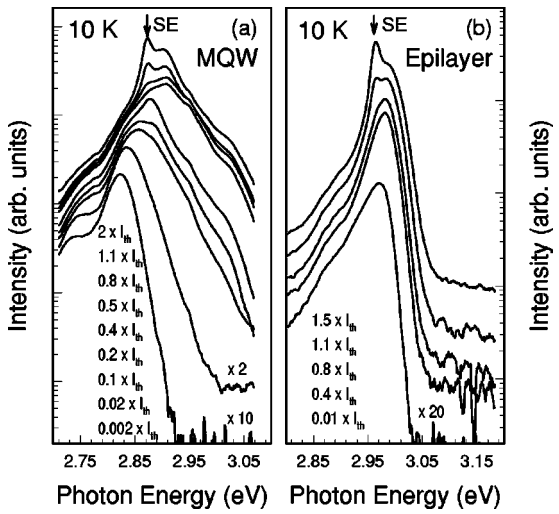

FIG. 2. Evolution of InGaN emission spectra from below to above SE threshold, I_{th}, at 10 K for (a) an InGaN/GaN MQW and (b) an InGaN epilayer. The emission was collected in a surface emission geometry. I_{th} for the MQW and epilayer was found to be $\sim$170 and 130 kW/cm^2, respectively, for the experimental conditions. A large blueshift of the emission is cleary seen with increasing excitation density for the MQW sample, showing band filling of localized states.

The lifetimes were also measured as a function of temperature. The rise in effective recombination lifetime with increasing temperature observed from 10 to $\sim$100 (20) K for the MQW (epilayer) is indicative of recombination dominated by radiative recombination channels, whereas the decrease in τ with increasing temperature for $T>100$ (20) K indicates the increasing dominance of nonradiative channels in the recombination process.[23,24] We observed that the MQW has a significantly larger τ than the epilayer for all temperatures studied, and the lifetimes of both are significantly larger than that of GaN epilayers and heterostructures.[20,25] This is attributed to suppression of nonradiative recombination by the localization of carriers at statistical potential fluctuations arising from the nonrandom nature of this alloy.

Figure 2 shows the evolution of the 10-K emission spectra with increasing excitation pump density (I_{exc}) for (a) the InGaN/GaN MQW and (b) the InGaN epilayer. The spectra shown in Fig. 2 were taken with an excitation energy of 3.49 eV and collected in a surface emission geometry to minimize the effects of reabsorption on the emission spectra. (The SE peak is due to a leak of the in-plane SE at the sample edge. No SE was observed from the middle of the sample in this geometry, indicating the high quality of the sample structure.[26]) The pump spot size was $\sim 1\,\mathrm{mm}^2$ and the excitation wavelength was the third harmonic of the Nd:YAG laser described above (355 nm). As I_{exc} is increased, the SPE peak of the MQW is observed to blueshift until it reaches $\sim$2.9 eV; after this point it is observed to increase only in intensity until the SE threshold is reached. The SE is seen to develop on the low-energy side of the SPE peak. The blueshift of the SPE with increasing I_{exc} is attributed to band filling of localized states due to the intense optical pump. With increasing I_{exc}, the filling level increases and the PL maximum shifts to higher energies until sufficient population inversion is achieved and net optical gain results in the observed SE peak. We see the I_{exc}-induced blueshift is significantly larger for the MQW than the epilayer ($\sim$ 12 nm for the MQW compared to $\sim$2 nm for the epilayer), further indicating that the potential fluctuations are significantly larger in the MQW than in the epilayer. For a large enough I_{exc}, the blueshift of the SPE with increasing I_{exc} stops, and further increases in I_{exc} result in SE, indicated by the arrows in Fig. 2. The SE peak is seen to grow out of the low-energy wing of the blueshifted SPE peak for both samples.

The Stokes shift between PL and PLE spectra, the redshift behavior with time (a rise in lifetime with decreasing emission energy), and the blueshift behavior with excitation energy are characteristic of the recombination of carriers localized at potential fluctuations. Moreover, the larger Stokes shift, longer lifetime, and larger SPE blueshift with excitation density for the MQW compared to those for the epilayer strongly reflect that the potential fluctuations are significantly larger in the MQW than in the epilayer. In general, the following effects are expected to lead to an emission shift in MQW's. They are not expected to be observed in epilayers: (i) the quantum confinement (blueshift), (ii) the built-in internal electric field (redshift), and (iii) the potential fluctuations (redshift) related to the presence of MQW interfaces. These potential fluctuations can be caused by alloy disorder, impurities, interface irregularities, and/or self-formed quantum dots in the QW active regions. As seen in Fig. 1, the redshift behavior is apparently larger than the blueshift in the MQW. This indicates that the MQW interfaces affect the emission properties mainly by means of (ii) and/or (iii). Although internal electric fields may be present in the MQW, potential fluctuations are more likely to dominate the emission properties of the sample considering the 3-nm-thick InGaN well widths of the MQW. In addition, the different growth conditions between the MQW and the epilayer may also affect the degree of potential fluctuations.

B. Nonlinear optical characteristics: Optical gain and pump-probe spectroscopy

Figure 3 shows the relevant 10-K PL, PLE, SE, and modal gain spectra for (a) the InGaN/GaN MQW and (b) the InGaN epilayer. Note that the x axis of (b) covers half that of (a). Representative SE spectra are shown (solid line) for pump density $I_{exc}=1.5I_{th}$ (I_{th} denotes the SE threshold) and an excitation spot size of $\sim 100\times 5000$ μm. Note that the SE peak is situated at the end of the absorption tail for both samples. The SE is seen to occur on the high-energy side of the low-power SPE peak for the MQW and slightly on the low-energy side for the epilayer. The modal gain (dotted line) was measured using the variable stripe excitation method of Shaklee and Leheny.[17,18] The spectra were taken with $I_{exc}\gg I_{th}$ for excitation length less than 200 μm to minimize reabsorption-induced distortions in the spectra. The modal gain maxima are 250 and 150 cm^{-1} for the MQW and the epilayer, respectively. We see that the SE peak for long excitation lengths (>5000 μm) is situated on the low-energy tail of the gain curve measured for small excitation lengths (<200 μm). This is explained by gain and absorption competition in the band-tail region of this alloy, where gain saturation with longer excitation lengths

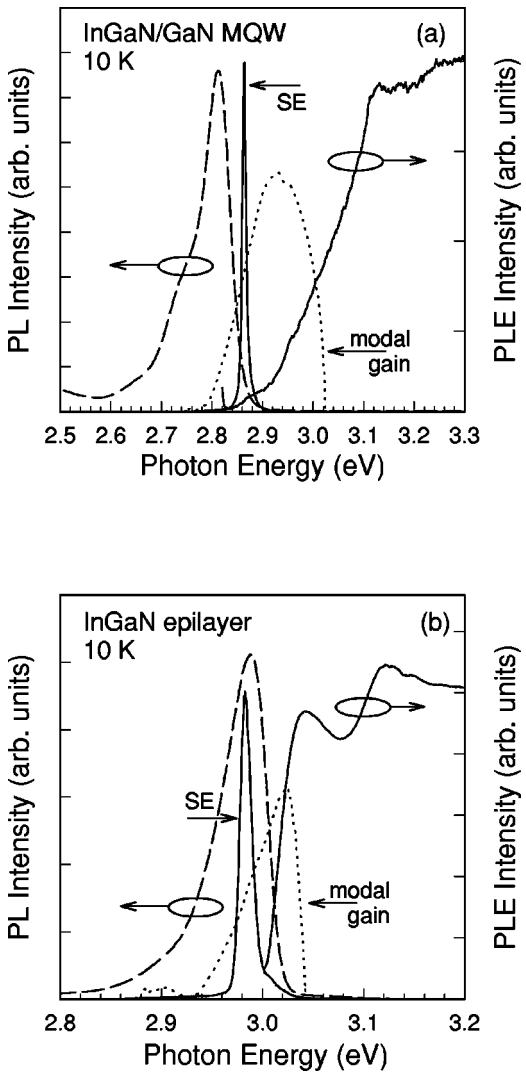

FIG. 3. PL (dashed lines), SE (solid lines), and modal gain (dotted lines) spectra taken at 10 K from (a) an InGaN/GaN MQW and (b) an InGaN epilayer. The SE and gain spectra were measured for excitation lengths of >5000 and <200 μm, respectively. The maximum modal gain is 250 and 150 cm^{-1} for the InGaN/GaN MQW's and InGaN epilayer, respectively. The low-density PLE spectra are also shown for reference.

combined with the background absorption tail leads to a redshift of the SE peak with increasing excitation length. The modal gain spectrum for the MQW is seen to be significantly broader ($\sim$24 nm FWHM) than that of the epilayer ($\sim$7 nm FWHM), although both peak significantly below the onset of the ''soft'' absorption edge.

The modal gain spectra as a function of above-gap optical excitation density are shown in Figs. 4(a) and 4(b) for the MQW and the epilayer, respectively. The excitation densities in Fig. 4 are given with respect to the SE threshold measured for long (>2000 μm) excitation lengths. A clear blueshift in the gain peak with increasing optical excitation is seen for the MQW. This blueshift was observed to stop for $I_{exc} > 12 I_{th}$. Further increases in I_{exc} result only in an increase in the modal gain maximum. The maxima of the gain spectra in Fig. 4(a) are redshifted by more than 160 meV with respect to the ''soft'' absorption edge of the InGaN well layers. The large shift in the gain maximum to higher energy

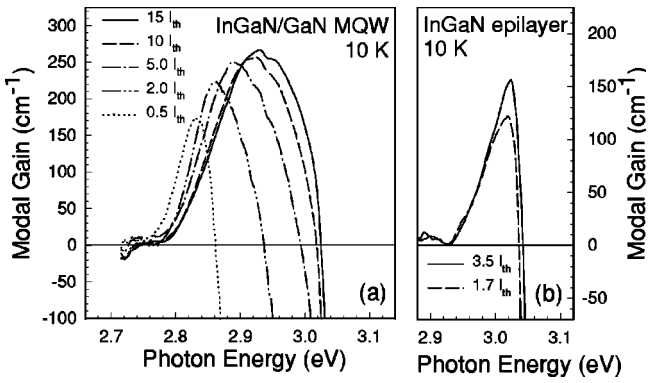

FIG. 4. 10-K modal gain spectra of (a) an InGaN/GaN MQW and (b) an InGaN epilayer as a function of above-gap optical excitation density. The excitation densities are given with respect to I_{th} measured for long (>2000 μm) excitation lengths. A clear blueshift in the gain maximum and gain/absorption crossover point is seen with increasing excitation density for the MQW sample. This trend is much less obvious for the InGaN epilayer. .

with increasing I_{exc} is consistent with band filling of localized states in the InGaN active layers. Similar behavior was observed at room temperature (RT). (We note that optical gain is observed only for photon energies below the mobility edge measured in energy-selective studies described later, giving further evidence that localized states are the origin of optical gain in the InGaN/GaN MQW structures.) The blueshift in the gain spectra of the InGaN epilayer is seen to be considerably smaller than that of the MQW. It was also observed to stop at considerably lower-excitation densities. The modal gain spectra of both samples correspond spectrally with the low-energy tail of the band-tail state absorption bleaching spectra, with the crossover from absorption to gain corresponding approximately with the maximum in the observed bleaching.

Figure 5 shows the absorption spectra of the InGaN epilayer near the fundamental absorption edge at 10 and 300 K, respectively. The oscillatory structure is a result of thin-film interference. With increasing excitation density of the above-gap pump pulse, the absorption coefficient in the band-tail region decreases significantly. This bleaching saturated for I_{exe} exceeding $\sim 2 MW/cm^2$ at 10 and 300 K. Similar behavior is observed for the MQW sample, the only difference being a larger spectral region exhibiting absorption bleaching due to the larger band tailing exhibited by the MQW sample. Differential absorption spectra, $\Delta\alpha(I_{exc}) = \alpha(I_{exc}) - \alpha(0)$, are also shown in Fig. 5 for clarity. We note that the induced transparency associated with the absorption bleaching is quite large, exceeding 3×10^4 cm^{-1} at both 10 and 300 K. The spectral region in which SE is observed is also indicated in Fig. 5. Clear features in the induced absorption bleaching spectra are seen to coincide with these spectral regions and are attributed to net optical amplification (gain) of the probe pulse. Again, similar behavior was observed for the InGaN/GaN MQW sample. Both $In_xGa_{1-x}N$-based structures were observed to exhibit markedly different behavior in the $\alpha(I_{exc})$ and $\Delta\alpha(I_{exc})$ spectra than has been observed in GaN thin films.[27,28]

Figure 6 shows the results of nanosecond nondegenerate optical pump-probe experiments performed on (a) the InGaN/GaN MQW and (b) the InGaN epilayer. Absorption

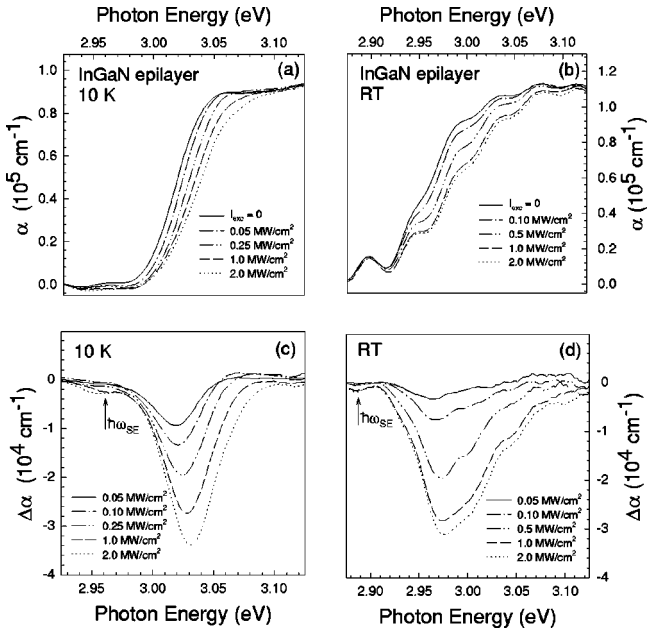

FIG. 5. Optical absorption spectra of an InGaN epilayer near the fundamental absorption edge at (a) 10 K and (b) 300 K as a function of above-gap optical excitation density. Differential absorption spectra, $\Delta\alpha(I_{exc})=\alpha(I_{exc})-\alpha(0)$, at (c) 10 K and (d) 300 K as a function of above-gap optical excitation for the sample. The SE energy is indicated by arrow for completeness.

bleaching of the band-tail states is clearly seen for both structures with increasing I_{exc}, where the bleaching is seen to cover the entire spectral range of the absorption tails of the samples. The bleaching is peaked at $\sim$3.02 eV for both samples, but is spectrally much broader for the MQW, consistent with its increased absorption tail. We note that the maximum in the absorption bleaching is significantly blue-shifted with respect to the luminescence maximum for both

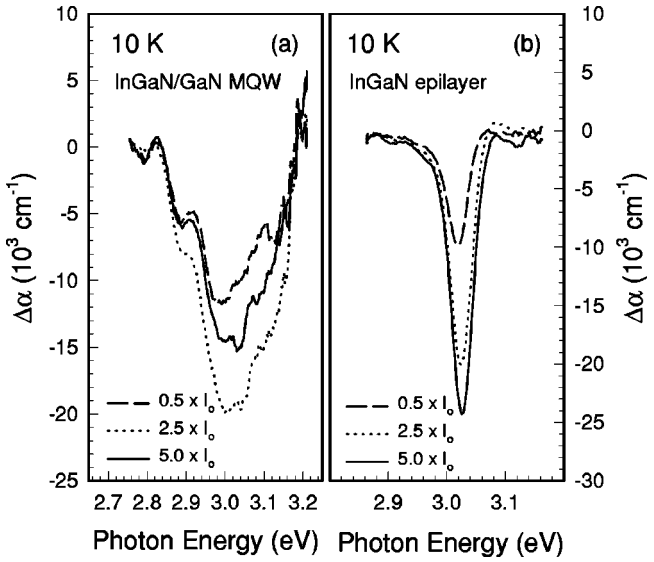

FIG. 6. 10-K nanosecond nondegenerate pump-probe experimental results for (a) an InGaN/GaN MQW and (b) an InGaN epilayer showing absorption bleaching ($\Delta\alpha$ negative) of band-tail states with increasing excitation density, I_{exc}. $\Delta\alpha(I_{exc})=\alpha(I_{exc})-\alpha(0)$ and $I_o=100$ kW/cm^2.

samples. This is explained by the intraband relaxation of photogenerated carriers, where the carriers are created with energies above the mobility edge (will be shown later), but are quickly caught in the potential wells of the band-tail states. Further intraband relaxation at low temperatures can then only occur by phonon-assisted tunneling to (deeper) neighboring potential wells or by further relaxation to lower energy states within the same wells until the potential minima are reached. Radiative recombination of these states is expected to be mainly from these potential minima, whereas higher-energy states are temporarily occupied by the relaxing carriers. The latter results in the observed absorption bleaching.

An interesting difference between the two structures is the behavior of the absorption bleaching as I_{th} is exceeded. As the pump density is increased, the bleaching is observed to increase for both samples, but as I_{th} is exceeded, the bleaching of the MQW tail states is seen to *decrease* significantly with increasing excitation, while the bleaching of the epilayer tail states continues to increase with increasing excitation density. This is shown in Figs. 6(a) and 6(b), where the dotted and dashed lines show the bleaching spectra for excitation densities below I_{th} and the solid lines show the bleaching spectra for excitation densities above I_{th}. The differences in behavior are explained by considering the recombination lifetimes shown in Figs. 1(a) and 1(b). Although radiative recombination from these samples occurs from potential minima, states of higher energy are temporarily occupied as the carriers excited by the pump beam relax, resulting in the observed bleaching peaked at higher energy than the luminescence maximums. The bleaching of the InGaN/GaN MQW decreases for excitation densities above I_{th} because of the fast depopulation of the states from which SE originates. Carriers with energies above the SE peak now have a much greater number of available lower-energy states. This, in turn, results in a decrease in states occupied at higher energies and, therefore, a decrease in the observed bleaching for excitation densities above I_{th}. This behavior has been previously observed in other materials where intrinsic disorder through compositional fluctuations has lead to similar carrier localization as is observed here.[29] The absence of the absorption bleaching decrease for excitation densities above I_{th} in the InGaN epilayer results from its short recombination lifetime ($\sim$0.8 ns) with respect to the pump pulse ($\sim$5 ns FWHM) [see Fig. 1(b)]. For the epilayer, the recombination lifetime is always significantly shorter than the pump pulse, leading to no noticeable reduction in the relaxation dynamics of the higher-energy band-tail states as I_{th} is exceeded. Therefore, no noticeable change in the bleaching behavior is observed. It is important to note that the modal gain shown in Figs. 3(a) and 3(b) (dotted lines) corresponds spectrally with the low-energy tail of the localized state absorption bleaching, with the crossover from absorption to gain corresponding approximately with the maximum in the observed bleaching for both samples, indicating that the gain originates from the localized states.The induced transparency maximum of the MQW sample corresponds spectrally to the mobility edge, as will be shown in Sec. III C. The experimental results presented in this section indicate that localized carriers responsible for band-tail state bleaching share the same recombination channels as the car-

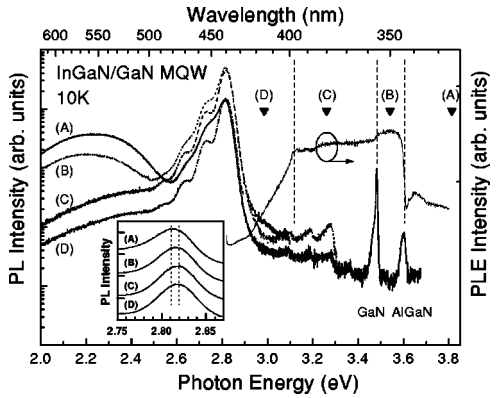

FIG. 7. Evolution of the PL emission of the InGaN/GaN MQW for excitation energies of (*A*) 3.81, (*B*) 3.54, (*C*) 3.26, and (*D*) 2.99 eV. Note the change in the intensity ratio of the main peak to the secondary peak between spectra. The inset shows a linear-scale plot of the normalized main emission spectra, which are vertically shifted for clarity. The excitation photon energies are indicated over the PLE spectrum for reference.

riers responsible for optical gain and SE in InGaN/GaN MQW's, providing strong evidence that optical gain originating from localized carriers exists in this material system.

C. Excitation energy dependence of SPE and SE

In this section, we present the results of energy-selective SPE and SE studies of the InGaN/GaN MQW's. SPE (SE) was observed for excitation photon energies over a wide spectral range above the SPE (SE) peak position.

1. SPE with various excitation energies: Energy-selective PL and PLE

Figure 7 shows 10-K InGaN-related PL spectra measured with four different excitation photon energies E_{exc} of (*A*) 3.81, (*B*) 3.54, (*C*) 3.26, and (*D*) 2.99 eV. Each E_{exc} is indicated over the PLE spectrum for reference. The InGaN-related *main peak* and *secondary peak* are shown with peak energies of 2.80 and $\sim$2.25 eV, respectively. The oscillations on the main PL peak are due to Fabry-Perot interference fringes. When E_{exc} varies from above (curve *A*) to below (curve *B*) the near-band-edge emission energy E_g of the AlGaN capping layer ($E_{g,\mathrm{AlGaN}}$), the relative intensity ratio of the main peak to the secondary peak noticeably changes. For $E_{exc}<E_{g,\mathrm{GaN}}$ (E_g of the GaN barriers), the secondary peak has nearly disappeared, while the main peak remains (curve *C*). When the excitation energy is further decreased to just above the InGaN main emission peak (curve *D*), no noticeable change is observed for the PL shape except for a decrease in the overall intensity of the emission. We now examine the changes in the main peak shape with excitation energy. The inset in Fig. 7 shows the normalized spectra for the main peak on a linear scale. We notice that, as the excitation energy is decreased (from curve *A* to curve *D*), the intensity of the lower-energy side of the main peak is reduced, whereas that of the higher-energy side is enhanced. This results in a $\sim$7-meV blueshift of the peak energy and a narrower spectral width for the main peak with decreasing excitation energy. These facts strongly reflect that the recombination mechanism of the InGaN-related emission is significantly affected by the excitation (or carrier generation) conditions, as can be seen later.

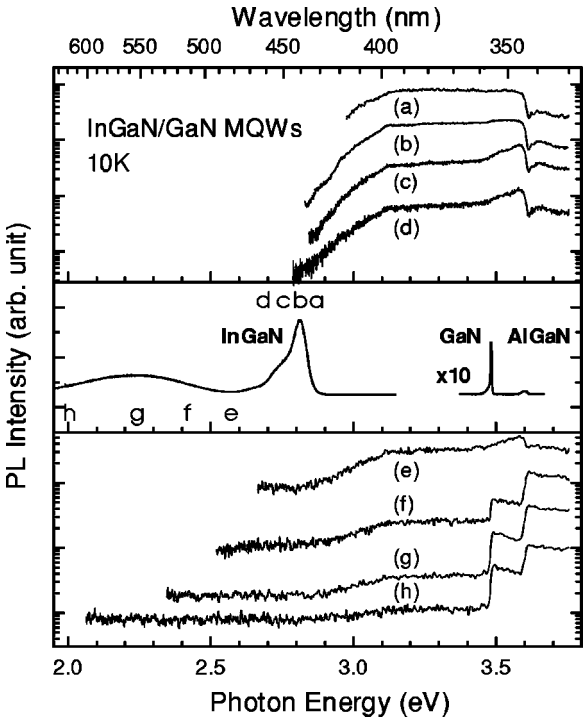

FIG. 8. 10-K PLE spectra taken at detection energies of (a) 2.87, (b) 2.81, (c) 2.75, (d) 2.68, (e) 2.57, (f) 2.41, (g) 2.24, and (h) 2.01 eV. The PL spectrum for an excitation energy of 3.81 eV is also shown for reference. The spectra are shifted in the vertical direction for clarity and the respective detection energies are marked. As the detection energy decreases, the contribution of the AlGaN capping layer noticeably increases. When the detection energy is lower than 2.24 eV, the contribution of the InGaN wells is almost negligible.

The upper part of Fig. 8 shows the 10-K PLE spectra for the InGaN-related main PL emission monitored at (*a*) 2.87, (*b*) 2.81, (*c*) 2.75, and (*d*) 2.68 eV. The PL spectrum for $E_{exc}=3.81$ eV is also shown in this figure for reference. When the PLE detection energy is set below the peak energy of the main emission (curves *c* and *d*), the contributions from the InGaN wells, the GaN barriers, and the AlGaN capping layer are clearly distinguishable, while for the detection energy above and at the peak position of the main emission $E_{p,\mathrm{InGaN}}$ (curves *a* and *b*), the PLE signal below $E_{g,\mathrm{AlGaN}}$ shows almost a constant intensity across the $E_{g,\mathrm{GaN}}$ region, indicating that the carrier generation in the InGaN rather than in the GaN plays an important role. In both cases, the PLE signal above $E_{g,\mathrm{AlGaN}}$ is suddenly diminished, obviously due to the absorption of the AlGaN capping layer. When the detection energy is below $E_{p,\mathrm{InGaN}}$ (curves *c* and *d*), the contributions of both the GaN and AlGaN regions are enhanced compared to the curves *a* and *b*: as the detection energy decreases, the PLE signal above $E_{g,\mathrm{GaN}}$ is monotonically raised with respect to the almost flat region of the PLE signal between 3.15 and 3.4 eV. These facts imply that for $E_{exc}>E_{g,\mathrm{GaN}}$, the lower-energy side of the InGaN main emission peak is governed mainly by carrier generation in the GaN barriers and subsequent carrier transfer to the InGaN wells. From the different PLE contributions for the

higher- and lower-energy sides of $E_{p,\mathrm{InGaN}}$, we can expect different recombination mechanisms for various excitation energies, as will be described later.

The lower part of Fig. 8 also shows the 10-K PLE spectra for the secondary peak taken for detection at (*e*) 2.57, (*f*) 2.41, (*g*) 2.24, and (*h*) 2.01 eV. When the detection energy is higher than 2.24 eV, the InGaN wells still partly contribute to the secondary-peak emission (curves *e* and *f*), while for the detection energy below 2.24 eV, the contribution of the InGaN wells almost disappears (curves *g* and *h*). Note that as the detection energy decreases, the contribution of the AlGaN capping layer is noticeably increased. These facts indicate that the main source of the secondary peak does not originate from the InGaN wells but originates predominantly from the AlGaN capping layer and partly from the GaN layers (consistent with the so-called *yellow luminescence band*). This observation was also confirmed by PL measurements using the 325-nm line of He-Cd laser with varying excitation intensities. As the excitation intensity increases, the relative emission intensity ratio of the InGaN main peak to the secondary peak increases. That is, the intensity of the main peak increases linearly, whereas that of the secondary peak saturates with increasing excitation intensity. This is another indication of the contribution of defect-related emission to the secondary peak. Therefore, we conclude that the main peak is due to the InGaN wells, while the secondary peak is mainly from the AlGaN capping layer and the GaN barriers rather than the InGaN wells. For $E_{exc}>E_{g,\mathrm{AlGaN}}$, most carriers are generated in the AlGaN capping layer and these photogenerated carriers partly migrate into the MQW region (corresponding to the main peak) and partly recombine via defect-related luminescence in the AlGaN layer itself and the GaN barriers (corresponding to the secondary peak).

Since the PLE observations in the frequency domain are closely related to the carrier dynamics in the time domain, we performed TRPL measurements at 10 K for different E_{exc} to clarify the temporal dynamics of the luminescence. The time-integrated PL spectra obtained from the TRPL experiments show the same behavior as observed in the above cw PL measurements for the InGaN-related main emission (see Fig. 7): a blueshift of the peak energy and a spectral narrowing of the lower-energy side as E_{exc} decreases from above $E_{g,\mathrm{AlGaN}}$ to below $E_{g,\mathrm{GaN}}$. The carrier recombination lifetime becomes longer with decreasing emission energy, and therefore, the peak energy of the emission shifts to the low-energy side as time progresses, as shown in Fig. 1. No significant change in lifetime at and above the peak energy position ($\tau_d \sim 12$ ns at the peak position) was observed when E_{exc} was varied. However, the peak position reached the lower-energy side faster for the $E_{exc}>E_{g,\mathrm{GaN}}$ case than for the $E_{exc}<E_{g,\mathrm{GaN}}$ case, and after ~ 20 ns, the peak position is almost the same for both cases. The starting peak position is lower for the $E_{exc}>E_{g,\mathrm{GaN}}$ case than for the $E_{exc}<E_{g,\mathrm{GaN}}$ case, so for the $E_{exc}>E_{g,\mathrm{GaN}}$ case, the redshifting behavior with time is smaller and most carriers recombine at relatively lower energies. The carriers generated from the GaN barriers (or AlGaN capping layer) migrate toward the InGaN wells, and the carrier transfer allows the photogenerated carriers to have a larger probability of reaching the lower-energy states at the MQW interfaces. This may be due to more binding and scattering of carriers by interface defects and roughness near the MQW interface region, since the carriers go through the MQW interfaces during the carrier transfer, enhancing trapping and recombination rates at the interface-related states. Therefore, the lower emission peak energy position and the spectral broadening to lower energies for $E_{exc}>E_{g,\mathrm{GaN}}$ indicate that the lower (or deeper) energy tail states are more related to the interface-related defects and roughness at the MQW interfaces than to the alloy fluctuations and impurities within the InGaN wells. For $E_{exc}<E_{g,\mathrm{GaN}}$, though, the carriers responsible for the emission are directly generated within the InGaN wells and thus recombine at relatively higher emission energies.

It should be noted that the PLE spectra of Fig. 8 show different slopes for $E_{exc}<3.0$ eV in curves *b*, *c*, and *d*. In order to investigate details of this phenomenon, we carried out energy-selective PL measurements using a femtosecond Ti:sapphire laser as a tunable excitation for $E_{exc}<E_{g,\mathrm{GaN}}$. The excitation photon energy from the frequency-doubled Ti:sapphire laser was tuned across the states responsible for the ''soft'' absorption edge of the InGaN layers. SPE was observed for excitation photon energies over a wide spectral range above the SPE peak position (2.8 eV at 10 K). As the excitation photon energy was tuned from just below the band gap of the GaN barrier layers to the high-energy side of the InGaN absorption edge, no significant changes in the SPE spectra were observed. The only change was a decrease in the emission intensity as the excitation photon energy was tuned below the higher-energy side of the ''soft'' InGaN absorption edge, consistent with the reduction in the absorption coefficient with decreasing photon energy in this spectral region. However, as the excitation photon energy was tuned below approximately 2.98 eV, significant changes in the SPE spectra were observed. For excitation photon energies below ~ 2.98 eV, emission from the low-energy wing of the main InGaN PL peak became more and more pronounced with decreasing excitation photon energy. This is illustrated in Figs. 9(a), 9(b), and 9(c). The spectra in Fig. 9 have been normalized at 2.79 eV for clarity. Figs. 9(b) and 9(c) clearly show the onset of this behavior to occur for excitation photon energies below approximately 2.98 eV. This behavior indicates that the transition from localized to extended band-tail states is located at ~ 2.98 eV. As such, this energy defines the ''mobility edge'' of the band-tail states in this structure, where carriers with energy above this value are free to migrate and those of lesser energy are spatially localized by (large) potential fluctuations in the InGaN layers.

The redshift in the SPE is explained as follows: when E_{exc} is higher than the mobility edge, the photogenerated carriers can easily populate the tail states by their migration, but their lifetimes are relatively short due to the presence of nonradiative recombination channels. As E_{exc} is tuned below the mobility edge, the nonradiative recombination rate is significantly reduced due to the capture of the carriers in small volumes. This increase in lifetime with decreasing E_{exc} results in increased radiative recombination from lower-energy states. The position of the mobility edge is seen to be ~ 180 meV above the SPE peak and $\sim$ 130 meV below the start of the InGaN absorption edge. Its spectral position indicates extremely large potential fluctuations are present in the InGaN active layers of the MQW, leading to carrier confinement and resulting in efficient radiative recombination.

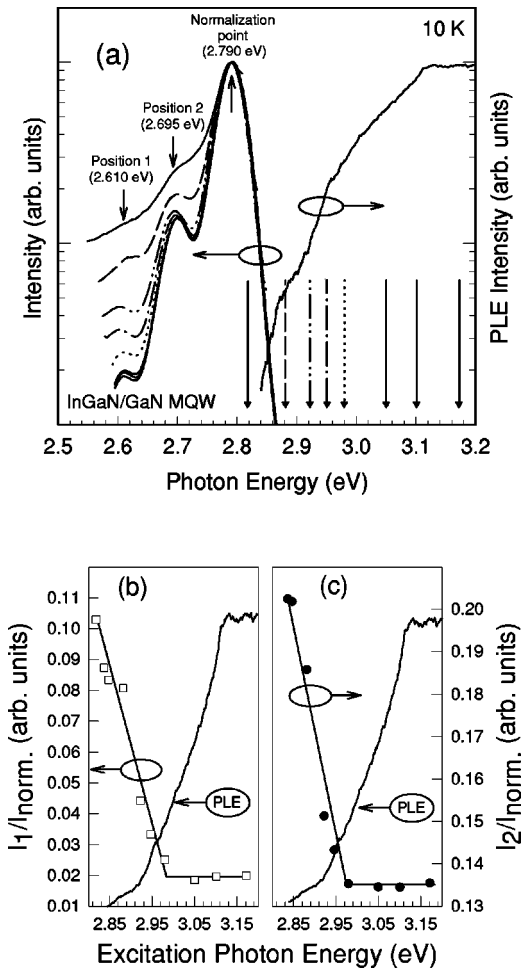

FIG. 9. (a) Spontaneous emission spectra from an InGaN/GaN MQW with 2×10^{18} cm^{-3} Si doping in the GaN barriers as a function of excitation photon energy. The excitation photon energy for a given spectrum is indicated by the corresponding arrow on the *x* axis. The spectra have been normalized at 2.79 eV for clarity. The absorption edge measured by PLE is also shown. (b) and (c) 10-K spontaneous emission intensity from an InGaN/GaN MQW at (b) 2.61 eV and (c) 2.695 eV relative to the peak emission intensity (at 2.79 eV) as a function of excitation photon energy. The solid lines are given only as a guide for the eye. A clear shift in the emission lineshape is seen for excitation photon energies below ~2.98 eV. The absorption edge measured by PLE is also given (solid line) for comparison.

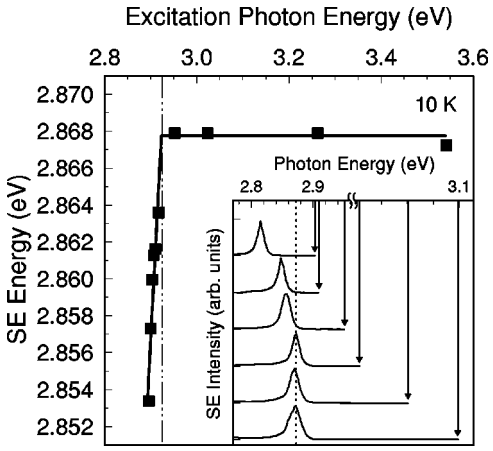

FIG. 10. SE peak position as a function of excitation photon energy, E_{exc}, for the InGaN/GaN MQW with 2×10^{18} cm^{-3} Si doping in the GaN barriers. ''Mobility edge'' type behavior is clearly seen in the SE spectra with decreasing E_{exc}. The solid lines are given only as a guide for the eye. The inset shows the redshift of the SE peak with decreasing E_{exc} as E_{exc} is tuned below the ''mobility edge'' for an InGaN/GaN MQW with undoped GaN barriers. The excitation photon energies for the given SE spectra are represented by the arrows in the inset. The dotted line in the inset is given as a reference for the unshifted SE peak position. The SE spectra have been normalized and displaced vertically for clarity.

2. Energy-selective optically pumped SE

To elucidate whether the CLO recombination responsible for the observed SPE is also responsible for SE in these materials, a similar experiment was performed using nanosecond optical pulses generated by a frequency doubled amplified dye laser, as described in Sec. II. (The excitation spot size was approximately 100×5000 μm.) The experiments were performed on both MQW's with Si-doped ($n\sim2\times10^{18}$ cm^{-3}) and undoped ($n<1\times10^{17}$ cm^{-3}) GaN barriers. Figure 10 shows the behavior of the SE peak as E_{exc} is tuned from above $E_{g,\mathrm{AlGaN}}$ to below the absorption edge of the InGaN active layers. As E_{exc} is tuned to lower energies, no noticeable change is observed in the SE spectrum until E_{exc} crosses a certain value, at which point the SE spectrum redshifts quickly with decreasing E_{exc}. The inset of Fig. 10 illustrates the SE spectra position change as a function of E_{exc} for the InGaN/GaN MQW with undoped GaN barrier layers, while the main part of Fig. 10 gives the behavior of the SE peak for the doped MQW, which is presented in Fig. 11. The SE peak position is seen to be relatively insensitive to E_{exc} for energies higher than ~2.925 eV, but as E_{exc} is tuned below this value, the SE peak position is seen to redshift quickly. This redshift of the emission for excitation photon energies below a certain value is consistent with the mobility edge behavior observed for the SPE, as described above. The behavior of the SE peak is due to enhanced population inversion at lower energies as the carriers are confined more efficiently with decreasing E_{exc}. The mobility edge measured in these experiments lies ~110 meV above the SPE peak, ~62 meV above the SE peak, and ~185 meV below the absorption edge of the InGaN well regions. The location of the mobility edge with respect to the SPE and SE peaks further indicates that large potential fluctuations are present in the InGaN active regions, resulting in strong carrier localization. This explains the efficient radiative recombination (stimulated and spontaneous) observed from these structures as well as the low temperature sensitivity of the SE, as will be shown in Sec. III E 2.

As a measure of the coupling efficiency of the exciting photons to the gain mechanism responsible for the SE peak, I_{th} was measured as a function of E_{exc}. A comparison between this and the coupling efficiency obtained for the SPE peak measured by PLE is given in Fig. 11, where $1/I_{th}$ is plotted as a function of E_{exc} to give a better measure of the coupling efficiency and afford an easier comparison to the results of PLE measurements. Four distinct slope changes are seen in the PLE spectrum. The first, at ~3.12 eV, marks the beginning of the ''soft'' absorption edge of the InGaN-active region, whereas the other three, located at ~2.96 eV, 2.92

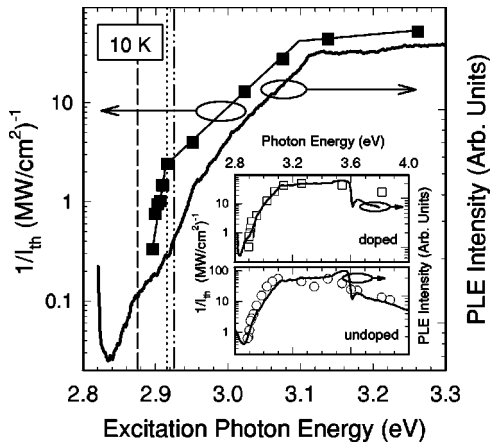

FIG. 11. Inverse SE threshold as a function of excitation photon energy E_{exc} (solid squares) shown in comparison with the results of low-power PLE experiments (solid line) for the Si-doped InGaN/GaN MQW. The band-filling maximum is included in the plot (dashed line) as is the ''mobility edge'' shown in Fig. 9 (dashed-dotted line). The dotted line shows the excitation photon energy at which the SE threshold is found to increase quickly with decreasing E_{exc}. The inset shows the same comparison over a wider energy range for both the undoped and Si-doped InGaN/GaN MQW's, illustrating the similarities over the entire energy range.

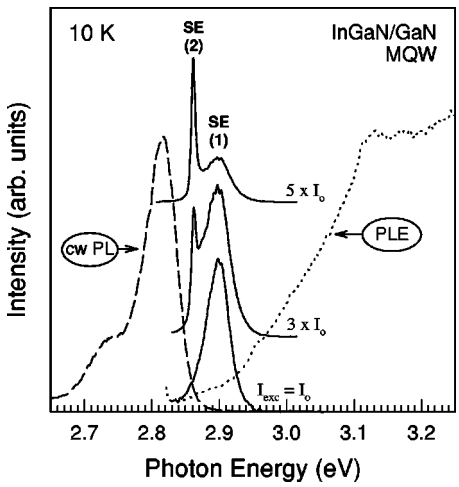

FIG. 12. 10-K SE spectra (solid lines) from an InGaN/GaN MQW sample subjected to several excitation densities, where $I_0 = 100$ kW/cm^2. The low power PL (dashed line) and PLE (dotted line) spectra are also shown for comparison. The SE spectra have been normalized and displaced vertically for clarity.

eV, and 2.87 eV suggest varying degrees of localization. The change in $1/I_{th}$ at ~ 3.1 eV is due to a decrease in the absorption coefficient below the absorption edge, and is an expected result. The change in $1/I_{th}$ at ~ 2.92 eV (indicated by the dotted line) is coincident with a slope change in the PLE spectrum and is attributed to a significant decrease in the effective absorption cross section for excitation photon energies below the mobility edge (indicated by the dashed-dotted line). The band filling maximum (shown by a dashed line in Fig. 11) corresponds to the slope change at 2.875 eV in the PLE spectrum in Fig. 11. The inset of Fig. 11 shows the same comparison over a wider energy range for both the Si-doped and undoped MQW's. A strong correlation between the SE threshold and PLE measurements is clearly seen over the entire range for both samples. The correlation between the high-density behavior presented here and the cw PLE results indicates that carrier localization plays a significant role in both the SPE and SE processes.

Furthermore, we note that optical gain of the InGaN/GaN MQW ($n \sim 2 \times 10^{18}$ cm^{-3}) (see Fig. 4) is observed only for photon energies below the mobility edge and the induced transparency maximum of the same MQW (see Fig. 6) corresponds spectrally to the mobility edge measured in the energy-selective optical experiments. These facts strongly indicate that localized carriers responsible for band tail state bleaching share the same recombination channels as the carriers responsible for optical gain and SE in InGaN/GaN MQW's, providing strong evidence that optical gain originates from localized carriers in this material system.

D. Excitation length dependence of SE

With the recent observation of two different SE peaks from $In_xGa_{1-x}N$/GaN MQW's grown by Nichia Chemical Industries[30] we see the possibility that some of the varied results reported in the literature may stem from slightly different experimental conditions, which are shown here to result in significant changes in the SE behavior. We report the results of a detailed study of the SE behavior of these two SE peaks as a function of excitation length (L_{exc}) and I_{exc} and illustrate dramatically different SE behavior in $In_xGa_{1-x}N$ MQW's for relatively small changes in the experimental conditions. The observation of these two distinct SE peaks from $In_xGa_{1-x}N$/GaN MQW's grown under different conditions by separate research groups suggests this SE behavior is a general property of present state-of-the-art $In_xGa_{1-x}N$ based blue laser diodes. As such, a better understanding of the SE and lasing behavior of these structures is important for the development and optimization of future laser diode structures.

Typical power-dependent emission spectra at 10 K for the InGaN/GaN MQW sample with barrier Si doping of $n = 2 \times 10^{18}$ cm^{-3} are shown in Fig. 12 for an excitation length $L_{exc} = 1300$ μm. At low I_{exc}, we observe a broad SPE peak at ~ 2.81 eV, consistent with low power cw PL spectra. As I_{exc} is increased, a new peak emerges at ~ 2.90 eV [designated here as SE peak (1)] and grows superlinearly with increasing I_{exc}. If we continue to increase I_{exc}, we observe another new peak at ~ 2.86 eV [designated here as SE peak (2)] which also grows superlinearly with increasing I_{exc}. SE peak (1) is observed to be the statistical distribution of a multitude of narrow (~ 0.1 nm) emission lines. Both SE peaks (1) and (2) originate on the high-energy side of the low-power SPE peak (given by the dashed line in Fig. 12) and are redshifted by more than 30 nm below the ''soft'' absorption edge. Both SE peaks were found to be highly TE polarized, with a TE to TM ratio of ~ 200. SE peak (2) was studied in previous sections and attributed to stimulated recombination of localized states through nanosecond nondegenerate optical pump-probe experiments showing that the onset of SE has a direct impact on the bleaching dynamics of the band-tail states in these samples (see Sec. III B), and through the use of energy-selective optically pumped SE

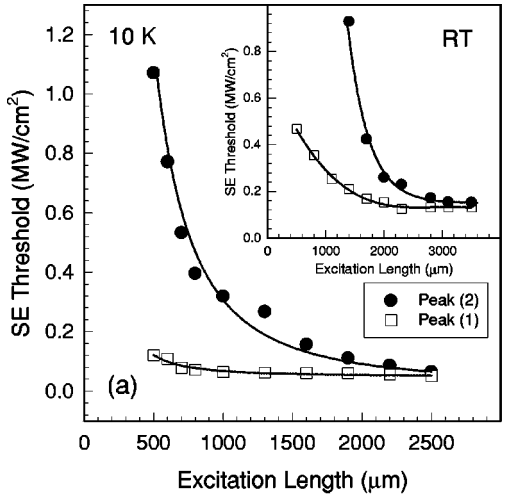

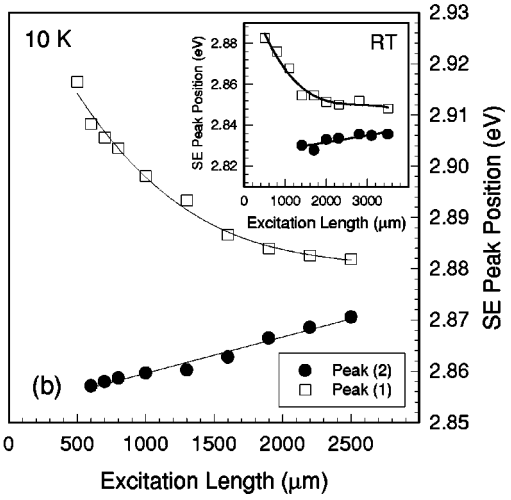

FIG. 13. (a) SE threshold as a function of excitation length for SE peaks (1) and (2) at 10 K for an InGaN/GaN MQW. (b) Peak position of SE peaks (1) and (2) as a function of excitation length at 10 K for an InGaN/GaN MQW. The inset shows the behavior observed at room temperature. The solid lines are given only as guides for the eye.

studies showing ''mobility edge'' type behavior in the SE spectra as the excitation photon energy is varied (see Sec. III C 2).

Figure 13(a) shows the I_{th} of SE peaks (1) and (2) as a function of L_{exc}. We note that I_{th} for peak (2) is larger than that of peak (1) for all excitation lengths employed, but approaches that of peak (1) with increasing L_{exc} in an asymptotic fashion. The high I_{th} of peak (2) with respect to peak (1) and its increased presence for longer L_{exc} suggest that it results from a lower gain process than that of peak (1). Figure 13(b) shows the peak positions of SE peak (1) and SE peak (2) as a function of L_{exc} at 10 K. For $L_{exc}<500$ μm, only SE peak (1) is observed with a peak emission photon energy at 10 (300) K of $\sim$2.92 (2.88) eV and an I_{th} of $\sim$100 (475) kW/cm^2. As I_{exc} is increased and/or L_{exc} is increased, a new SE peak [SE peak (2)] emerges at 2.86 (2.83) eV at 10 (300) K. The peak positions were measured for I_{exc} fixed relative to the SE thresholds of the respective peaks; i.e., $I_{exc}=2I_{th}$. As L_{exc} is increased, SE peak (1) shifts to lower energies due to a reabsorption process, while the SE peak (2) position is observed to be weakly dependent on L_{exc}. The apparent blueshift of SE peak (2) with increasing L_{exc} seen in Fig. 13(b) is a result of the experimental conditions. Since the I_{th} of SE peak (2) is a strong function of L_{exc}, the peak positions shown for small L_{exc} are for I_{exc} considerably higher than for large L_{exc}. The slight redshift of SE peak (2) with increasing I_{exc} due to many-body effects and lattice heating (see Fig. 14) then manifests itself as the apparent blueshift seen in Fig. 13(b). The same phenomenon is observed at 300 K, as shown in the inset of Fig. 13(b). The redshift of SE peak (1) with increasing L_{exc} can be explained by gain and absorption competition in the ''soft'' absorption edge of the InGaN-active regions, where gain saturation with longer L_{exc} combined with the background absorption tail leads to the observed redshift. The fact that SE peak (2) does not experience a reabsorption-induced redshift with increasing L_{exc} is explained by the significant reduction of the absorption tail in this spectral region (see Fig. 12).

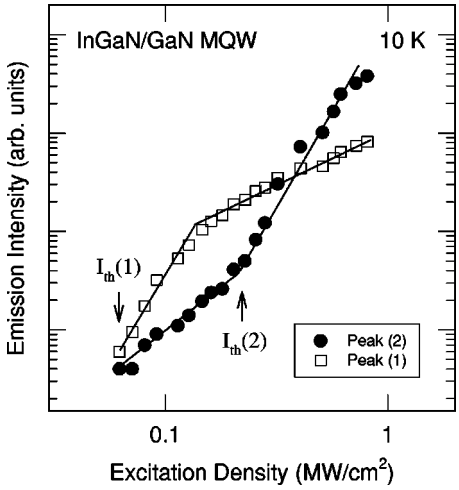

FIG. 14. Emission intensity of SE peaks (1) and (2) as a function of optical excitation density at 10 K, illustrating gain competition between SE peaks (1) and (2). The excitation length is 1300 μm. The respective SE thresholds of SE peaks (1) and (2) are indicated for completeness. The solid lines are given only as guides for the eye.

The gain saturation behavior of SE peak (1) is consistent with the observation of Kuball *et al.*[31] of a high-gain mechanism in the band-tail region of MQW's with similar active regions. The large spectral range exhibiting gain is explained by compositional fluctuations inside the active region. It is also consistent with the observation by Nakamura[32,33] that the external quantum efficiency of his cw blue laser diodes *decreases* with increasing cavity length. These similarities, combined with the relatively low I_{th} of SE peak (1) with respect to SE peak (2) and its similar spectral position with laser emission from diodes of similar structure,[34] suggest that lasing in current state-of-the-art cw blue laser diodes originates from the gain mechanism responsible for SE peak (1). Its origin may lie in an entirely different degree of carrier localization than is responsible for SE peak (2). Further experiments are needed to clarify this issue.

The dependence of the emission intensity of peaks (1) and (2) on I_{exc} is shown in Fig. 14 for $L_{exc}=1300$ μm at 10 K. The emission of peak (1) increases in a strongly superlinear

fashion ($\sim I_{exc}^{3.8}$) until the I_{th} of peak (2) is reached, at which point it turns linear, indicating that peak (2) competes for gain with peak (1). This is most likely a result of competition for carriers or reabsorption of the emitted photons. The presence of SE peak (2) is therefore seen to be deleterious to SE peak (1). The same process is observed at RT and for various excitation lengths. This gain competition may limit this material's performance in high-power laser diode applications, where increased driving current and/or longer cavity lengths may result in a shift in the dominant gain mechanism and a drastic change in the emission behavior.

E. Temperature dependence of SPE and SE

Recently, a temperature-induced luminescence blueshift was observed in $In_xGa_{1-x}N$ single QW light-emitting diodes, and an involvement of band-tail states was proposed.[35,36] However, the correlation between the temperature-induced anomalous emission behavior with its carrier dynamics is not well understood. In this section, we present the results of temperature-dependent PL, integrated PL intensity, TRPL, and the results of optically pumped SE studies well above the RT (175–575 K).

1. Carrier dynamics of temperature-induced emission shift

In general, the temperature-induced fundamental energy gap shrinkage of GaN and $In_xGa_{1-x}N$ epilayers can be described by the Varshni empirical equation,[37] $E_g(T)=E_g(0)-\alpha T^2/(\beta+T)$, where $E_g(T)$ is the transition energy at a temperature T, and α and β are known as Varshni thermal coefficients. Previously, from photoreflectance studies, the parameters $\alpha=8.32\times10^{-4}$ eV/K (10×10^{-4} eV/K) and $\beta=835.6$ K (1196 K) for the GaN Γ_9^v-Γ_7^c ($In_{0.14}Ga_{0.86}N$) transition were obtained.[38,39] For simplicity, Varshni thermal coefficients obtained from the GaN and $In_{0.14}Ga_{0.86}N$ transitions[38,39] were used for the E_g estimation of the $Al_{0.07}Ga_{0.93}N$ and $In_{0.18}Ga_{0.82}N$ layers, respectively. The temperature-dependent PL peak shift for the GaN and $Al_{0.07}Ga_{0.93}N$ layers was consistent with the estimated energy decrease of about 65 meV between 10 and 300 K, whereas the InGaN-related PL emission did not follow the typical temperature dependence of the energy gap shrinkage, as will be shown later.

Figure 15 shows the evolution of the InGaN-related PL spectra for (a) an InGaN/GaN MQW and (b) an InGaN epilayer over a temperature range from 10 to 300 K. As the temperature increases from 10 K to T_I, where T_I is 70 (50) K for the MQW (epilayer), E_{PL} redshifts 19 (10) meV. This value is about five times as large as the expected band-gap shrinkage of $\sim$4 (2) meV for the MQW (epilayer) over this temperature range.[39] For a further increase in temperature, the PL peak blueshifts 14 (22.5) meV from T_I to T_{II}, where T_{II} is 150 (110) K for the MQW (epilayer). By considering the estimated temperature-induced band-gap shrinkage of $\sim$13 (7) meV for the MQW (epilayer), the actual blueshift of the PL peak with respect to the band-edge is about 27 (29.5) meV over this temperature range. When the temperature is further increased above T_{II}, the peak positions redshift again. From the observed redshift of 16 (45) meV and the expected band-gap shrinkage of $\sim$43 (51) meV from T_{II} to 300 K for the MQW (epilayer), we estimate an actual blueshift of the PL peak relative to the band-edge to be about 27 (6) meV in this temperature range.

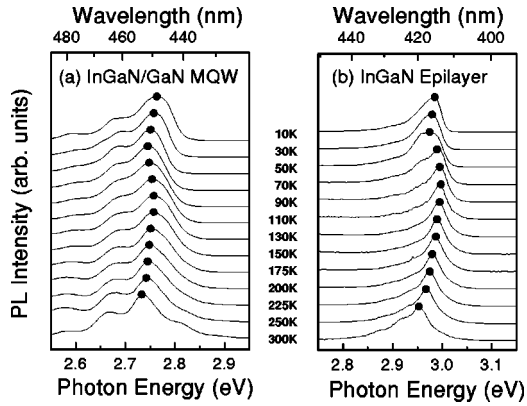

FIG. 15. Typical InGaN-related PL spectra for (a) an InGaN/GaN MQW and (b) an InGaN epilayer in the temperature range from 10 to 300 K. The main emission peak of both samples shows an S-shaped shift with increasing temperature (solid circles). All spectra are normalized and shifted in the vertical direction for clarity. Note that the turning temperature from redshift to blueshift is about 70 and 50 K for the InGaN/GaN MQW and the InGaN epilayer, respectively.

Figure 16 shows an Arrhenius plot of the normalized integrated PL intensity for the InGaN-related PL emission over the temperature range under investigation. The total luminescence intensity from this sample is reduced by only one order of magnitude from 10 to 300 K, indicating a high PL efficiency even at high temperatures. At $T>70$ K, the integrated PL intensity is thermally activated with an activation energy of about 35 meV. In general, the quenching of the luminescence with temperature can be explained by thermal emission of the carriers out of a confining potential with an activation energy correlated with the depth of the confining potential. Since the observed activation energy is much less than the band offsets as well as the band-gap difference between the wells and the barriers, the thermal quenching of the InGaN-related emission is *not* due to the thermal activation of electrons and/or holes from the InGaN wells into the GaN barriers. Instead, the dominant mechanism leading to the quenching of the InGaN-related PL is due to thermionic emission of photogenerated carriers out of the potential minima caused by potential fluctuations, such as alloy and interface fluctuations, as will be discussed later.

To elucidate the kinetics of carrier recombination, we performed TRPL measurements over the same temperature range. Figure 17 shows E_{PL}, the relative energy difference (ΔE) between E_{PL} and E_g at each temperature, and the decay times (τ_d) monitored at the peak energy, lower-energy side, and higher-energy side of the peak as a function of temperature. A comparison clearly shows that the temperature dependence of ΔE and E_{PL} is strongly correlated with the change in τ_d. For both the InGaN/GaN MQW and the InGaN epilayer, we found an overall increase of τ_d with increasing temperature for $T<T_I$, in qualitative agreement with the temperature dependence of radiative recombination.[23,24] As shown in Sec. III A, in this temperature range, τ_d becomes longer with decreasing emission energy, and hence, the peak energy of the emission shifts to the low-energy side as time proceeds. This behavior is a charac-

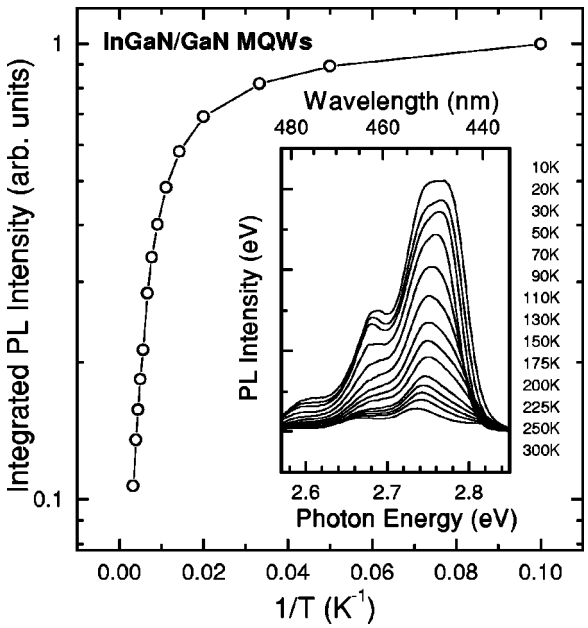

FIG. 16. Normalized integrated PL intensity as a function of $1/T$ for the InGaN-related emission in the InGaN/GaN MQW's (open circles). The inset shows InGaN-related PL spectra for the temperature range from 10 to 300 K. An activation energy of $\sim$35 meV is obtained from the Arrhenius plot.

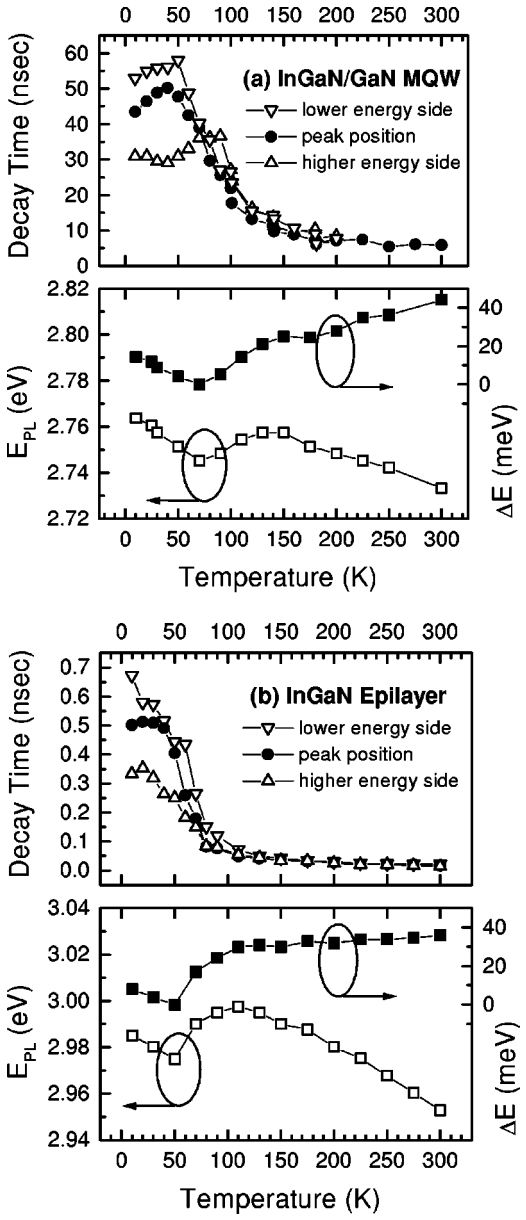

FIG. 17. InGaN-related PL spectral peak position E_{PL} (open squares) and decay time τ_d as a function of temperature in (a) an InGaN/GaN MQW and (b) an InGaN epilayer. ΔE (closed squares) represents the relative energy difference between E_{PL} and E_g at each temperature. The minimum value of ΔE is designated as zero for simplicity. Note that the lower energy side of the PL peak has a longer lifetime than the higher energy side below a certain temperature T_I, while there is no difference between lifetimes monitored above, below, and at the peak energy above T_I, where T_I is about 70 (50) K for the MQW (epilayer). This characteristic temperature T_I is also where the turnover occurs from redshift to blueshift of the InGaN PL peak energy with increasing temperature. A blueshift behavior of emission peak energy with increasing temperature is still seen at room temperature for the InGaN/GaN MQW, while this behavior is much less for the InGaN epilayer.

teristic of localized carriers, which in this case is most likely due to alloy fluctuations (and/or interface roughness in the MQW's). As the temperature is further increased beyond T_I, the lifetime of the MQW (epilayer) quickly decreases to less than 10 (0.1) ns and remains almost constant between T_{II} and 300 K, indicating that nonradiative processes predominantly affect the emission. This is further evidenced by the fact that there is no difference between the lifetimes monitored above, below, and at the peak energy for $T>T_I$, in contrast to the observations for $T<T_I$. This characteristic temperature T_I is also where the turnover occurs from redshift to blueshift for ΔE and E_{PL} with increasing temperature. Furthermore, in the temperature range between T_I and T_{II}, where a blueshift of E_{PL} is detected, τ_d dramatically decreases from 35 to 8 (0.4 to 0.05) ns for the MQW (epilayer). Above T_{II}, where a redshift of E_{PL} is observed, no sudden change in τ_d occurs for both the MQW and the epilayer.

From these results, the InGaN-related recombination mechanism for different temperature ranges can be explained as follows: (i) For $T<T_I$, since the radiative recombination process is dominant, the carrier lifetime increases, giving the carriers more opportunity to relax down into lower-energy tail states caused by the inhomogeneous potential fluctuations before recombining. This reduces the higher-energy side emission intensity, and thus, produces a redshift in the peak energy position with increasing temperature. (ii) For $T_I<T<T_{II}$, since the dissociation rate is increased and other nonradiative processes become dominant, the carrier lifetimes decrease greatly with increasing temperature and also become independent of the emission energies. Thus, due to the decreasing lifetime, these carriers recombine before reaching the lower-energy tail states. This gives rise to an apparent broadening of the higher-energy side emission and leads to a blueshift in the peak energy. (iii) For $T>T_{II}$, since nonradiative recombination processes are dominant and the lifetimes are almost constant [in contrast to case (ii)], the photogenerated carriers are less affected by the change in carrier lifetime so that the blueshift behavior becomes smaller. Note that the slope of ΔE is very sensitive to the

change in τ_d with temperature for both the InGaN epilayer and the InGaN/GaN MQW's. Since this blueshift behavior is smaller than the temperature-induced band-gap shrinkage in this temperature range, the peak position exhibits an overall redshift behavior. Consequently, the change in carrier recombination mechanism with increasing temperature causes the S-shaped redshift-blueshift-redshift behavior of the peak energy for the main InGaN-related emission. It should be noted that we observed similar temperature-induced S-shaped emission behavior for both the InGaN epilayers and the InGaN/GaN MQW's, even though τ_d of the latter is about two orders of magnitude longer than that of the former. This fact strongly reflects that the anomalous temperature-induced emission shift mainly depends on the change in carrier recombination dynamics rather than the absolute value of τ_d.

2. High-temperature optically pumped SE

As we have mentioned in Sec. III D, SE peak (1) at 10 K for the InGaN/GaN MQW sample with barrier Si doping of $n=2\times10^{18}$ cm^{-3} was observed to be a statistical distribution of a multitude of narrow ($\sim$0.1 nm) emission lines (see Fig. 12). No noticeable broadening of these narrow emission lines in SE peak (1) was observed as the temperature was tuned from 10 K to 575 K. This is illustrated in Fig. 18. Dotted lines represent the broad SPE spectra taken at pumping densities approximately half that of the SE threshold for each temperature. As we raise I_{exc} above I_{th}, a considerable spectral narrowing occurs (solid lines in Fig. 18). The emission spectra are comprised of many narrow peaks of less than 0.1 nm FWHM. The major effect of the temperature change from 200 K [Fig. 18(a)] to 450 K [Fig. 18(c)] was a shift of the SPE and SE peaks toward lower energy.

We found that an increase in the temperature leads to a decrease in PL intensity. This indicates the onset of efficient losses and a decrease in quantum efficiency of MQW's. At high temperatures, only a small fraction of carriers reach conduction-band minima, and most of them recombine nonradiatively. The modal gain depends only on radiatively recombining carriers. Therefore, the temperature increase efficiently decreases modal gain and leads to an increase in the SE threshold. To evaluate the number of carriers that recombine radiatively, we studied the integrated PL intensity as a function of excitation power for different temperatures, as shown in Fig. 19(a). For the temperature range studied, we found that under low excitation densities, the integrated intensity I_{integ} from the sample almost linearly increases with pump density I_p (i.e. $I_{integ}\propto I_p^g$, where $g=0.8$–1.3), whereas at high excitation densities, this dependence becomes superlinear (i.e., $I_{integ}\propto I_p^b$, where $b=2.2$–3.0). The excitation pump power at which the slope of I_{integ} changes corresponds to I_{th} at a given temperature. Interestingly, the slopes of I_{integ} below and above the I_{th} do not significantly change over the temperature range involved in this study. This reflects that the mechanism of SE in InGaN/GaN MQW's at RT remains the same as we raise the temperature to hundreds of degrees above RT.

The temperature dependence of I_{th} is shown in Fig. 19(b) (solid dots). SE was observed throughout the entire temperature range studied, from 175 K to 575 K. The SE threshold was measured to be $\sim$25 kW/cm^2 at 175 K, $\sim$55 kW/cm^2 at 300 K, and $\sim$300 kW/cm^2 at 575 K, and roughly followed

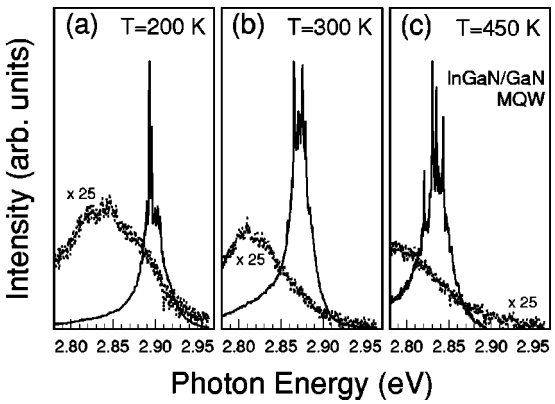

FIG. 18. SE spectra of SE peak (1) for an InGaN/GaN MQW with barrier Si doping of $n=2\times10^{18}$ cm^{-3} at (a) 200 K, (b) 300 K, and (c) 450 K, illustrating that SE peak (1) is composed of a multitude of narrow ($<$0.1 nm) peaks that do not noticeably broaden with increasing temperature. These SE spectra were collected for excitation densities twice the SE threshold for the respective temperatures. The SPE spectra (dotted lines) are also shown for excitation densities half of the SE threshold at each temperature. The SE spectra have been normalized for clarity.

an exponential dependence. It is likely that such a low I_{th} is due to the large localization of carriers in MQW's. The solid line in Fig. 19(b) represents the best result of the least-squares fit of the experimental data to the empirical form $I_{th}(T)=I_o\exp(T/T_c)$ for the temperature dependence of the I_{th}. The characteristic temperature, T_c, was estimated to be 162 K in the temperature range of 175–575 K for this sample. This value of characteristic temperature is considerably larger than the near RT values reported for laser structures based on other III-V (Refs. 40 and 41) and II-VI (Refs. 42 and 43) materials, where the relatively small values of T_c were a strong limiting factor for high-temperature laser operation. Such a low sensitivity of the I_{th} to temperature changes in $In_xGa_{1-x}N$/GaN MQW's opens up enormous opportunities for their high-temperature applications. The laser diodes with $In_xGa_{1-x}N$/GaN lasing mediums can potentially operate at temperatures exceeding RT by a few hundred degrees Kelvin.

IV. DISCUSSION

The main objective of this paper is to discuss the responsible SPE and SE mechanisms in state-of-the-art blue-light-emitting $In_xGa_{1-x}N$/GaN MQW structures grown on sapphire. Recently, the influence of IEF and CLO on optical properties in both GaN/$Al_xGa_{1-x}N$ and $In_xGa_{1-x}N$/GaN QW's has been reported by several authors. One notes that the emission characteristics may be influenced by the material system (e.g., GaN/$Al_xGa_{1-x}N$ or $In_xGa_{1-x}N$/GaN) and alloy composition in the active region (e.g., $x<0.1$ or $x>0.15$ in $In_xGa_{1-x}N$/GaN QW's), as well as other structural properties (e.g., well thickness, doping concentration, number of QW's, etc.). The $In_xGa_{1-x}N$/GaN QW samples used in this work have sufficient In composition to move emission wavelengths into the blue region of the visible spectrum. In the case of $In_xGa_{1-x}N$/GaN QW's, unfortunately, both IEF and CLO effects may be generally enhanced with increasing In alloy composition (at least up to 50%), which makes it

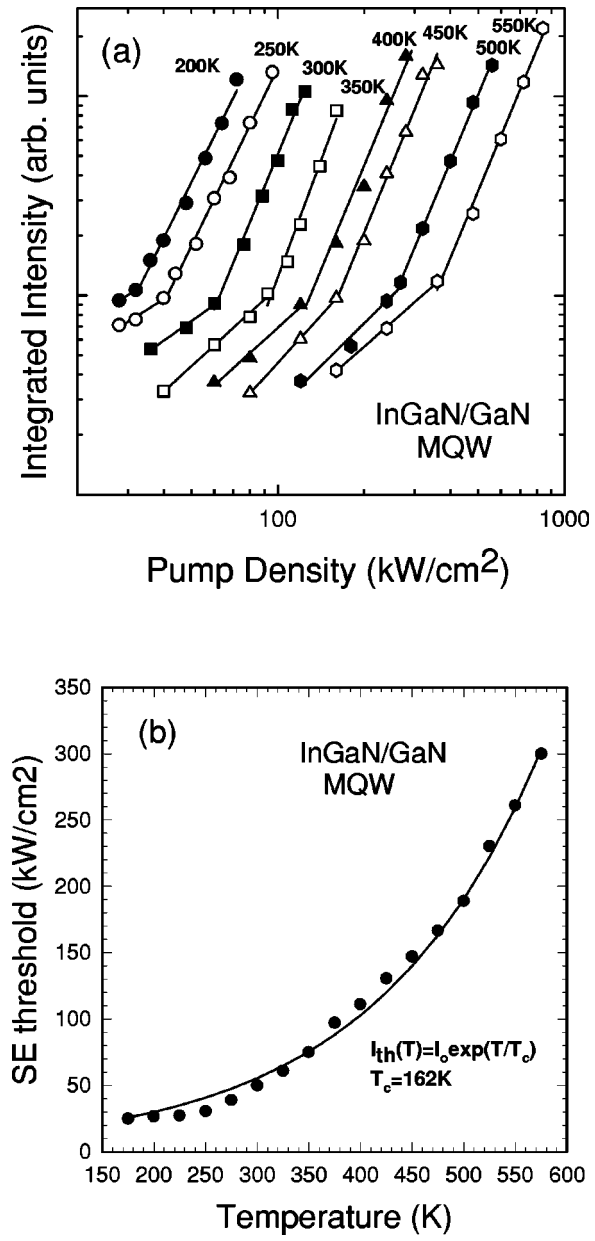

FIG. 19. (a) Integrated intensity of InGaN/GaN MQW emission as a function of optical excitation density for different temperatures. The slope change from 0.8–1.3 to 2.2–3.0 indicates the transition from SPE to SE. (b) Temperature dependence of the SE threshold in the temperature range of 175–575 K for the InGaN/GaN MQW sample. The solid line represents the best least-squares fit to the experimental data (solid dots). A characteristic temperature of 162 K is derived from the fit over the temperature range of 175–575 K.

difficult to extract one effect from the other. Although one may try to exclude (or reduce) the influence of alloy compositional fluctuation by introducing sample configurations with nonalloy (or small-alloy) active regions, such as $GaN/Al_xGa_{1-x}N$ QW's, the results obtained from these samples may not necessarily be extended to the case of samples with rather large-alloy active regions, such as the blue-emitting $In_xGa_{1-x}N/GaN$ QW's presented in this work.

First, we note that most of the earlier works by several groups using optical properties to assign the responsible recombination mechanism mainly relied on some of the following experimental observations (as shown in Sec. III A): (a) a Stokes shift between the emission peak energy and absorption edge (Fig. 1), (b) a redshift behavior of emission with decay time (equivalently, a rise in decay time with decreasing emission energy) (Fig. 1), and (c) a blueshift behavior of emission with increasing optical power density (Fig. 2). Interestingly, although many groups observed similar experimental findings for the QW's, their interpretations on the observations have been quite different and the observations have been used to support both the IEF and CLO models. The main reason is that these observations may be—at least qualitatively—explained in terms of both the IEF and CLO models,[6,12,44] as follows. In the presence of an IEF, the electrons and holes are separated to opposite sides within the $In_xGa_{1-x}N$ wells. An overlap between the wave functions of these spatially separated electrons and holes allows their radiative recombination within the wells at a lower energy than if there is no IEF [observation (a)]. When carriers are either optically or electrically generated, the generated carriers partially screen the IEF, and thus, separated electrons and holes come spatially closer together. Accordingly, the effective band gap that was reduced by the IEF begins to approach the band gap without the IEF [observation (c)]. As time proceeds, the generated carriers recombine, and hence, the IEF screened by the generated carriers recovers [observation (b)]. In the presence of CLO, on the other hand, large potential fluctuations result in the emission from localized carriers at potential minima while the absorption mostly occurs at the average potential energy [observation (a)]. As the excitation power increases, the carriers can fill the band-tail states of the fluctuations and thus the average emission energy increases [observation (c)]. As time proceeds, the carriers go down to the lower band-tail states and shows the redshift behavior with time [observation (b)]. Accordingly, the trend of the above experimental observations (a), (b), and (c) can be plausibly explained by the IEF *and/or* CLO models, especially for the case of $In_xGa_{1-x}N/GaN$ QW's. Because of this ambiguity, therefore, one could not strongly argue which effect is the predominant emission mechanism without more direct experimental evidence. Although we do not rule out the influence of IEF in the $In_xGa_{1-x}N/GaN$ QW's, most of our observations in this study cannot be explained in the framework of the IEF (EHP) alone for SPE (SE), without the consideration of strong CLO, as follows.

The nonlinear optical properties of band-tail states in highly excited InGaN/GaN MQW's have been investigated using variable-stripe gain spectroscopy and nanosecond nondegenerate optical pump-probe spectroscopy (see Sec. III B). The experimental results were compared with those obtained from an InGaN layer of comparable indium composition. We observed (d) a large blueshift behavior in the gain maximum with increasing pump power in variable stripe gain spectroscopy (Figs. 3 and 4) and (e) an absorption bleaching (induced transparency) behavior with increasing pump power density in nondegenerate pump-probe experiments (Figs. 5 and 6). Optical gain studies showed substantial blueshifts in the gain maximum with increasing above-gap optical excitation. The blueshifting behavior was attributed to the filling of localized band-tail states due to the intense optical pump. The large spectral region covered by the blueshift evidences the large magnitude of the potential fluctuations present in the InGaN active layers. Nanosecond nondegenerate optical

pump-probe spectroscopy of the near band edge transitions shows strong bleaching of band-tail states with increasing above-gap optical excitation. The magnitude of the bleaching was found to be significantly affected by the onset of SE, indicating the carriers responsible for bleaching and SE share the same recombination channels. These results provide strong evidence for the dominance of localized state recombination in the gain and SE spectra of the $In_xGa_{1-x}N$/GaN heterostructures.

Excitation energy dependence studies of SPE and SE supply important information about the energy boundary between localized and delocalized states (see Sec. III C). We observed (f) different PL spectra for different excitation photon energies above and below the GaN band gap with confirmation through an evolution of PLE spectra as a function of detection energy in InGaN emission (Figs. 7 and 8), (g) a mobility edge type behavior in SPE spectra as the excitation photon energy is tuned across the states responsible for the broadened absorption edge of the InGaN-active regions (Fig. 9), and (h) a mobility edge type behavior in not only SE spectra, but also the SE threshold with varying excitation photon energy across the InGaN absorption band tail (Figs. 10 and 11). Based on observation (f), we believe that the lower-energy tail states are more related to the interface-related defects and roughness at the MQW interfaces rather than to alloy fluctuations and impurities within the InGaN wells. We note that SPE and SE peak energies are well below the mobility edge obtained in the energy selective SPE and SE experiments [(g) and (h)], respectively. The relative position of the mobility edge with respect to the absorption edge and the SPE and SE peak positions indicates the emission originates from carriers localized at low-energy band-tail states due to extremely large potential fluctuations in the InGaN-active layers of the MQW's. The results on SE threshold density as a function of excitation energy is very consistent with the PLE spectra, indicating the coupling efficiency of the exciting photons to the gain mechanism responsible for the SE peak is correlated with that of the SPE mechanism. The correlation between the high-density behavior and the low-density cw PLE results indicates that CLO plays a significant role in both the SPE and SE processes.

To investigate SE features further, the dependence of SE on excitation length in InGaN/GaN MQW structures was measured (see Sec. III D). (i) Two distinctly different SE peaks were observed with different dependencies on excitation length (Fig. 12). (j) The high-energy SE peak exhibits a strong redshift with increasing excitation length due to competition between an easily saturable gain mechanism and a background absorption tail, while the lower-energy SE peak does not exhibit this reabsorption-induced redshift with increasing excitation length (Fig. 13). (k) The presence of the lower energy SE peak has been shown to be detrimental to the higher energy SE peak due to gain competition in the InGaN-active region (Fig. 14). This competition may prove to be an obstacle in the design of $In_xGa_{1-x}N$-based high-power laser diodes, where high current densities and/or long cavity lengths can lead to a shift in the dominant gain mechanism and a change in emission characteristics.

The temperature dependence of the emission features gives important insight into the recombination mechanism responsible for the SPE and SE (see Sec. III E). We showed (l) an abnormal temperature-induced ''S-shaped'' emission shift and its carrier dynamics as a function of temperature (Figs. 15, 16, and 17), (m) a narrow FWHM of SE spectra and its temperature invariance in the temperature range of 175–575 K (Fig. 18), and (n) an extremely low SE threshold density and rather low temperature dependence of SE threshold (Fig. 19). The integrated PL intensity and carrier lifetime as a function of temperature reveal that the InGaN-related emission is strongly affected by the change in carrier recombination dynamics with increasing temperature. The anomalous temperature-induced emission behavior is attributed to the inhomogeneity and carrier localization in the MQW's. Therefore, the InGaN-related SPE features are significantly affected by different carrier recombination dynamics that vary with temperature, because of band-tail states arising from large In alloy fluctuations, layer thickness variations, and/or defects in the MQW's. We note that observation (l) is not explainable in the framework of IEF alone without consideration of CLO. Increasing the temperature would strongly affect the recombination features by means of thermal filling of band tail states in the presence of CLO. In other words, thermally populated carriers at band-tail states recombine with different average emission peak energies, depending on the change in carrier lifetime and their thermal energy. Note that, even at RT, the temperature-induced blueshift behavior of the SPE peak of InGaN/GaN MQW's is still observable, and the emission peak energy is still lower than the mobility edge, as shown by the energy selective PL experiments in Sec. III C. This suggests that CLO plays an important role in InGaN/GaN MQW structures even at RT operation. The SE spectra observations (m) and (n) further indicate that the SE is strongly related to CLO, rather than EHP. We studied SE in optically pumped InGaN/GaN MQW's in the temperature range of 175–575 K. The characteristic temperature derived from the temperature dependence of the SE threshold was 162 K. The integrated emission intensity versus pumping density was examined at different temperatures. We observed that the slopes of the integrated emission intensity below and above the SE threshold are not sensitive to temperature changes. We showed that a low SE threshold and a weak temperature sensitivity of the SE threshold make $In_xGa_{1-x}N$ MQW's an attractive material for the development of laser diodes operable well above RT.

Finally, we emphasize that our observations (a), (b), (c), (f), (g), and (l) are consistent with the CLO model for the SPE mechanism, while (f), (g), and (l) cannot be explained by IEF alone without introducing the CLO effect. We also stress that our SE observations (d), (e), (h), (i), (j), (k), (m), and (n) strongly indicate that the responsible mechanism for SE is also CLO, rather than EHP. Accordingly, we demonstrate that our observations are more consistent with the CLO model than the IEF and EHP models for SPE and SE, respectively.

V. CONCLUSIONS

We have systematically investigated both the spontaneous and stimulated emission properties of blue-light-emitting $In_xGa_{1-x}N$/GaN MQW structures on sapphire using various linear and nonlinear optical techniques. Our findings in the range from low (for spontaneous emission) to high (for

stimulated emission) optical power densities are consistently understandable in the context of localization of photogenerated carriers associated with strong potential fluctuations. The excitation power, excitation photon energy, excitation length, and temperature dependence of the emission show carrier localization behaviors for both spontaneous and stimulated emission, demonstrating the presence and important role of strong inhomogeneous potential fluctuations in the $In_xGa_{1-x}N$-active region and heterointerface vicinity.

The internal electric field effect (due to spontaneous and/or piezoelectric polarization) alone does not explain the observed spontaneous emission features (e.g., mobility-edge-type behavior and an anomalous temperature dependence). In addition, the comprehensive experimental results strongly indicate that the stimulated emission has the same microscopic origin as the spontaneous emission, i.e., radiative recombination of localized states. Consequently, we conclude that carriers localized at potential fluctuations in $In_xGa_{1-x}N$-active layers and interfaces plays a key role in not only spontaneous but also stimulated emission of state-of-the-art blue-light-emitting $In_xGa_{1-x}N/GaN$ quantum-well structures.

ACKNOWLEDGMENTS

This work was supported by AFOSR, ARO, ONR, and DARPA.

[1] S. Nakamura, M. Senoh, N. Iwasa, S. Nagahama, T. Yamada, and T. Mukai, Jpn. J. Appl. Phys., Part 2 **34**, L1332 (1995).
[2] S. Nakamura, M. Senoh, S. Nagahama, N. Iwasa, T. Yamada, T. Matsushita, Y. Sugimoto, and H. Kiyoku, Appl. Phys. Lett. **69**, 4056 (1996).
[3] D. L. Smith and C. Mailhiot, Phys. Rev. Lett. **58**, 1264 (1987).
[4] F. Bernardini and V. Fiorentini, Phys. Rev. B **56**, R10 024 (1997).
[5] T. Takeuchi, S. Sota, M. Katsuragawa, M. Komori, H. Takeuchi, H. Amano, and I. Akasaki, Jpn. J. Appl. Phys., Part 2 **36**, L382 (1997).
[6] J. S. Im, H. Lollmer, J. Off, A. Sohmer, F. Scholz, and A. Hangleiter, Phys. Rev. B **57**, R9435 (1998).
[7] R. Langer, J. Simon, O. Konovalov, N. Pelekanos, A. Barski, and M. Leszczynski, MRS Internet J. Nitride Semicond. Res. **3**, 46 (1998).
[8] E. S. Jeon, V. Kozlov, Y.-K. Song, A. Vertikov, M. Kuball, A. V. Nurmikko, H. Liu, C. Chen, R. S. Kern, C. P. Kuo, and M. G. Craford, Appl. Phys. Lett. **69**, 4194 (1996).
[9] S. Chichibu, T. Azuhata, T. Sota, and S. Nakamura, Appl. Phys. Lett. **69**, 4188 (1996).
[10] P. Perlin, V. Iota, B. A. Weinstein, P. Wiśniewski, T. Suski, P. G. Eliseev, and M. Osiński, Appl. Phys. Lett. **70**, 2993 (1997).
[11] Y. H. Cho, G. H. Gainer, A. J. Fischer, J. J. Song, S. Keller, U. K. Mishra, and S. P. Denbaars, Appl. Phys. Lett. **73**, 1370 (1998).
[12] P. Lefebvre, J. Allègre, B. Gil, A. Kavokine, H. Mathieu, W. Kim, A. Salvador, A. Botchkarev, and H. Morkoç, Phys. Rev. B **57**, R9447 (1998).
[13] Y. Narukawa, Y. Kawakami, M. Funato, Sz. Fujita, Sg. Fujita, and S. Nakamura, Appl. Phys. Lett. **70**, 981 (1997).
[14] Y. Narukawa, Y. Kawakami, Sz. Fujita, Sg. Fujita, and S. Nakamura, Phys. Rev. B **55**, R1938 (1997).
[15] Y. H. Cho, F. Fedler, R. J. Hauenstein, G. H. Park, J. J. Song, S. Keller, U. K. Mishra, and S. P. DenBaars, J. Appl. Phys. **85**, 3006 (1999).
[16] X. H. Yang, T. J. Schmidt, W. Shan, J. J. Song, and B. Goldenberg, Appl. Phys. Lett. **66**, 1 (1995).
[17] K. L. Shaklee and R. F. Leheny, Appl. Phys. Lett **18**, 475 (1971).
[18] K. L. Shaklee, R. E. Nahory, and R. F. Lehny, J. Lumin. **7**, 284 (1973).
[19] H. X. Jiang, L. Q. Zu, and J. Y. Lin, Phys. Rev. B **42**, 7284 (1990).
[20] C. I. Harris, B. Monemar, H. Amano, and I. Akasaki, Appl. Phys. Lett. **67**, 840 (1995).
[21] C. K. Sun, S. Keller, G. Wang, M. S. Minsky, J. E. Bowers, and S. P. DenBaars, Appl. Phys. Lett. **69**, 1936 (1996).
[22] J. S. Im, V. Härle, F. Scholz, and A. Hangleiter, MRS Internet J. Nitride Semicond. Res. **1**, 37 (1996).
[23] B. K. Ridley, Phys. Rev. B **41**, 12 190 (1990).
[24] J. Feldmann, G. Peter, E. O. Göbel, P. Dawson, K. Moore, C. Foxon, and R. J. Elliott, Phys. Rev. Lett. **59**, 2337 (1987).
[25] W. Shan, X. C. Xie, J. J. Song, and B. Goldenberg, Appl. Phys. Lett. **67**, 2512 (1995).
[26] S. Bidnyk, T.J. Schmidt, G.H. Park, and J.J. Song, Appl. Phys. Lett. **71**, 729 (1997).
[27] T. J. Schmidt, J. J. Song, Y. C. Chang, B. Goldenberg, and R. Horning, Appl. Phys. Lett. **72**, 1504 (1998).
[28] T. J. Schmidt, Y. C. Chang, and J. J. Song, Proc. SPIE **3419**, 61 (1998).
[29] T. Breitkopf, H. Kalt, C. Klingshirn, and A. Reznitsky, J. Opt. Soc. Am. B **13**, 1251 (1996).
[30] T. Deguchi, T. Azuhata, T. Sota, S. Chichibu, M. Arita, H. Nakanishi, and S. Nakamura, Semicond. Sci. Technol. **13**, 97 (1998).
[31] M. Kuball, E. S. Jeon, Y. K. Song, A. V. Nurmikko, P. Kozodoy, A. Abare, S. Keller, L. A. Coldren, U. K. Mishra, S. P. DenBaars, and D. A. Steigerwald, Appl. Phys. Lett. **70**, 2580 (1997).
[32] S. Nakamura and G. Fasol, *The Blue Laser Diode* (Springer, New York, 1997), Chap. 11.
[33] S. Nakamura, MRS Internet J. Nitride Semicond. Res. **2**, 5 (1997).
[34] M. P. Mack, A. Abare, M. Aizcorbe, P. Kozodoy, S. Keller, U. K. Mishra, L. Coldren, and S. P. DenBaars, MRS Internet J. Nitride Semicond. Res. **2**, 41 (1997).
[35] P. G. Eliseev, P. Perlin, J. Lee, and M. Osiński, Appl. Phys. Lett. **71**, 569 (1997).
[36] K. G. Zolina, V. E. Kudryashov, A. N. Turkin, and A. E. Yunovich, MRS Internet J. Nitride Semicond. Res. **1**, 11 (1996).
[37] Y. P. Varshni, Physica (Utrecht) **34**, 149 (1967).
[38] W. Shan, T. J. Schmidt, X. H. Yang, S. J. Hwang, J. J. Song, and B. Goldenberg, Appl. Phys. Lett. **66**, 985 (1995).
[39] W. Shan, B. D. Little, J. J. Song, Z. C. Feng, M. Schurman, and R. A. Stall, Appl. Phys. Lett. **69**, 3315 (1996).
[40] H. Shoji, Y. Nakata, K. Mukai, Y. Sugiyama, M. Sugawara, N. Yokoyama, and H. Ishikawa, Appl. Phys. Lett. **71**, 193 (1997).

[41] P. D. Floyd and D. W. Treat, Appl. Phys. Lett. **70**, 2493 (1997).
[42] H. Jeon, J. Ding, A. V. Nurmikko, W. Xie, D. C. Grillo, M. Kobayashi, R. L. Gunshor, G. C. Hua, and N. Otsuka, Appl. Phys. Lett. **60**, 2045 (1992).
[43] J. M. Gaines, R. R. Drenten, K. W. Haberern, T. Marshall, P. Mensz, and J. Petruzzello, Appl. Phys. Lett. **62**, 2462 (1993).
[44] Y. Narukawa, Y. Kawakami, Sg. Fujita, and S. Nakamura, Phys. Rev. B **59**, 10 283 (1999).